NUREG/CR-1873
ANL-80-111

Distribution
Codes: R2 and
R4

ARGONNE NATIONAL LABORATORY
9700 South Cass Avenue
Argonne, Illinois 60439

STUDY OF TWO-FLUID MODEL AND INTERFACIAL AREA

by

M. Ishii and K. Mishima

Reactor Analysis and Safety Division

December 1980

Prepared for the Division of Reactor Safety Research
Office of Nuclear Regulatory Research
U. S. Nuclear Regulatory Commission
Washington, D. C. 20555
Under Interagency Agreement DOE 40-550-75

NRC FIN No. A2026-1

STUDY OF TWO-FLUID MODEL
AND INTERFACIAL AREA

by

M. Ishii and K. Mishima

ABSTRACT

The interfacial transfer terms are the weakest link in a two-fluid-model formulation, because of considerable difficulties in terms of experimentation as well as modeling. However, these terms are of supreme importance for a two-fluid model in determining phase interactions between liquid and vapor. In view of these, the interfacial transfer terms have been studied in detail and new constitutive relations have been developed. The interfacial terms are proportional to the interfacial area and driving force; therefore these two effects are modeled separately. In addition, new flow-regime criteria that are appropriate for a two-fluid model are proposed.

NRC
FIN No. FIN Title

A2026-1 Phenomenological Modeling of Two-phase Flow in Water Reactor Safety

TABLE OF CONTENTS

TABLE OF CONTENTS

LIST OF FIGURES

LIST OF FIGURES

LIST OF TABLES

NOMENCLATURE

NOMENCLATURE

A_d	Projected area of a particle
A_i	Surface area of a particle
a_i	Interfacial area per unit volume
B_d	Volume of a particle
B_d^*	Volume associated with induced mass
b	Half height of an ellipsoidal particle
C_{an}	Roughness parameter for annular flow
C_{ct}	Roughness parameter for churn-turbulent flow
C_D	Drag coefficient
C_M	Induced mass coefficient
C_0	Distribution parameter
D	Tube diameter
D_b	Diameter of a slug bubble
E	Aspect ratio, ratio of the maximum vertical dimension to maximum horizontal dimension of a particle
F_D	Drag force
F_v	Virtual mass force
$f\left(\left[\frac{\partial p}{\partial z}\right]_{fr}, v\right)$	Function of frictional pressure drop and velocity for interfacial area
$f(\alpha_d)$	Given function of α_d
g	Gravity
H_k	Enthalpy of k phase
h	Distance from the top of a bubble
h_{k_i}	Heat-transfer coefficient at interface
j_k	Volumetric flux of k phase
L	Pitch of a slug flow
L_b	Length of a slug bubble
L_s	Length scale, reciprocal of interfacial area per unit volume
M_{ik}	Interfacial force for k phase
$\overline{m_k}$	Mean mass transfer per unit area for k phase
N_d	Number density of dispersed phase
N_{Eo}	Eotvos number
N_{Re}	Particle Reynolds number
$N_{\mu f}$	Viscosity number
P_k	Pressure of k phase
$\bar{q}_k$	Mean conduction heat flux
q_k^t	Turbulent heat flux
q_{ki}''	Interfacial heat flux
r_D	Drag radius
r_d	Particle radius
r_p	Radius along the horizontal axis of an ellipsoidal particle

NOMENCLATURE

NOMENCLATURE

r_s	Surface radius
r_{sm}	Sauter mean radius
r_v	Equivalent radius (volume)
T_i	Temperature at interface
T_k	Bulk temperature based on the mean enthalpy of k phase
t	Time
v_k	Velocity of k phase
v_r	Relative velocity
z	Axial coordinate
α_b	Void fraction in a slug bubble section
α_{fd}	Liquid-drop volume fraction in gas core alone
α_{gs}	Average void fraction in the liquid slug and film
α_k	Void fraction of k phase
Γ_k	Mass source for k phase
$\Delta\rho$	Absolute value of density difference
θ	Wake angle of a cup bubble
λ	Parameter for a special convective derivative
μ_k	Viscosity of k phase
ν_k	Kinematic viscosity of k phase
ξ	Integral variable in Basset term
ρ_k	Density of k phase
σ	Surface tension
τ_i	Average interfacial shear force
$\bar{\bar{\tau}}_k$	Average viscous stress for k phase
τ_k^t	Turbulent stress for k phase
Φ	Velocity potential
Φ_k	Energy dissipation for k phase
Ω	Potential of external force

Subscripts

b	Bubble
c	Continuous phase
D	Drag
d	Dispersed phase
f	Liquid phase
fr	Friction
g	Gas phase
i	Value at interface
k	k phase (k = 1, 2; k = c, d; k = f, g; or k = b or m)
m	Mixture

STUDY OF TWO-FLUID MODEL AND INTERFACIAL AREA

by

M. Ishii and K. Mishima

EXECUTIVE SUMMARY

In predicting two-phase flow transients in nuclear reactors under various accident conditions, a two-fluid model is very important because of its detailed description of thermohydraulic transients and phase interactions. The interfacial transfer terms in the two-fluid model specify the rate of phase change, momentum exchange, and heat transfer at interfaces. Previous studies have indicated that, unless phase-interaction terms are accurately modeled in the two-fluid model, the complicated model does not necessarily warrant accurate solutions. In the present state of the art, the weakest link in the two-fluid-model formulation is the modeling of the constitutive relations for the interfacial transfer terms. In view of this, the interfacial transfer terms for the two-fluid formulation have been studied in detail here. The interfacial transfer of mass, momentum, and energy is proportional to the interfacial area and driving force. These two effects are considered separately.

Geometrical effects on the interfacial transfers are taken into account primarily by the interfacial area concentration. An extensive literature survey on existing experimental data has been completed, and a preliminary modeling effort for the interfacial area has been carried out. Basically four flow regimes, namely, dispersed (bubbly or droplet), slug, churn-turbulent, and annular flows, have been modeled separately, and general characteristics of the prediction have been discussed. The models show the importance of the existence and size of small fluid particles for all flow regimes. Although a number of data exist, the ranges covered by these data are far short of being sufficient for reactor applications. The flows studied fall into the slug, churn, and annular-flow regimes at moderate liquid fluxes (3-50 cm/s). For these regimes, the observed interfacial area concentration was in the range of 1-10 cm^2/cm^3. The effect of the density ratio or pressure on the interfacial areas has not been studied experimentally. However, the most important shortcoming of existing data may be the lack of information for developing flows. In view of fundamental difficulties encountered in modeling entrance and rapid transient flow under reactor accident conditions, considerable efforts should be made to develop some data base for interfacial areas for such flows.

The modeling of the momentum interaction term is essentially completed. It was assumed that the general drag force could be expressed by a linear combination of three terms. These are the standard-drag, virtual-mass, and Basset forces. Each of these three forces are modeled separately. The standard drag

correlation was obtained from the postulated drag-similarity law based on the mixture viscosity. The results for dispersed, slug, and churn-turbulent flows were compared to over 1000 data. Satisfactory agreements were obtained at wide ranges of concentration and Reynolds number.

Traditional flow-regime criteria based on the vapor and liquid volumetric fluxes may not be suitable to the two-fluid-model formulation, because these two parameters do not determine the void fraction uniquely. It has been concluded that for a two-fluid model, direct geometrical parameters such as the void fraction and interfacial area should be used in flow-regime criteria. From this point of view, new flow-regime criteria for both unrestricted and restricted flows have been developed. These new criteria can be compared to existing criteria under steady-state and fully developed flows by using relative velocity correlations obtained previously. The results showed satisfactory agreements.

I. INTRODUCTION

In predicting two-phase flow transients in nuclear reactors under various accident conditions, the interfacial transfer terms are among the most essential factors in the modeling. These interfacial transfer terms in a two-fluid model specify the rate of phase change, momentum exchange, and heat transfer at the interface between phases.

A two-fluid model[1-8] is formulated in terms of two sets of conservation equations governing the balance of mass, momentum, and energy of each phase. Since the macroscopic fields of one phase are not independent of these of the other phase, the interaction terms that couple the transport of mass, momentum, and energy of each phase across the interfaces appear in the field equation.[1] In the two-fluid-model formulation, the transport processes of each phase are expressed by their own balance equations. Therefore it is expected that the model can predict more detailed changes and phase interactions than a mixture model such as the drift-flux model.[9,10] In particular, for two-phase-flow problems involving a sudden acceleration of one phase, inertia terms of each phase should be considered separately by use of a two-fluid model.

Previous studies have indicated that, unless phase-interaction terms are accurately modeled in a two-fluid model, complications in the modeling do not necessarily warrant accurate solutions. For example, physically improper solutions and numerical instabilities are frequently encountered in the numerical solution of two-fluid models. A study by Lahey et al.[11] has demonstrated that virtual mass originating from momentum interaction between the two phases had a considerable effect on improving numerical stability and efficiency. It has also been suggested[12] that the interaction terms should include first-order time and spatial derivatives. Zuber[13] and others[14-16] indicated that the momentum-interaction term should have time and spatial derivatives and an integral term which expresses the short-time memory of the fluid. Another approach to achieving numerical stability is the inclusion of "artificial viscosity" in the numerical algorithm to damp out high-frequency oscillations occurring, possibly due to imprecise modeling. This approach is currently being followed by Amsden and Harlow[7] in their two-fluid digitial-computer codes. In spite of these shortcomings of a two-fluid model, there is, however, no substitute available for accurately modeling two-phase phenomena where two phases are not strongly coupled, as in an entrance flow or suddenly accelerating flow.

The weakest link in the two-fluid-model formulation is the constitutive equations for the interfacial interaction terms. The difficulties arise due to the complicated motion and geometry of interfaces in a general two-phase flow. Furthermore, these constitutive equations should be expressed by the macroscopic variables based on proper averaging. As has been shown in detail,[1,17] the interfacial transfer terms in a two-fluid model appear as averaging of local instant transfers of mass, momentum, and energy. Because these terms appear as source terms in the field equations, proper averaging alone is not sufficient to develop these constitutive equations. It is therefore essential

to clarify different physical mechanisms controlling these interfacial transfers as well as to identify important parameters that govern them.

The interfacial transfer terms are strongly related to the interfacial area concentration and to the local transfer mechanisms such as the degree of turbulence near interfaces.[1] Basically, the interfacial transport of mass, momentum, and energy is proportional to the interfacial area concentration, a_i, and to a driving force. This parameter, a_i, having the dimension of the reciprocal of length, characterizes the geometrical effects on the interfacial transfers. On the other hand, the driving forces for the interfacial transports depend on the local turbulence, transport properties, driving potentials, and some length scale at the interfaces. This length scale may be related to a transient time such as the particle residence time or to the interfacial area concentration and void fraction α.

The primary objective of the present research is to develop constitutive relations for interfacial transfer terms for a two-fluid model. In particular, the interfacial area concentration has been studied in detail here. An extensive literature survey on the existing experimental data[18-43] has been completed, and a preliminary analysis on the modeling of the interfacial area concentration has been carried out.

The void fraction and the interfacial area concentration characterize a geometrical configuration of a two-phase flow. In classical two-phase-flow analyses, the concept of the interfacial area concentration has not been explicitly introduced. Instead, two-phase flow-regime criteria and regime-dependent constitutive equations have been used extensively. Traditionally, flow regimes are identified from a flow-regime map based on the liquid and gas volumetric fluxes.[44-49] This approach may be suitable for slow transient and near fully developed conditions, where a mixture model such as the drift-flux model is sufficient.

However, in view of the practical applications of the two-fluid model to transient analysis of nuclear reactors under various accident conditions, several observations can be made. First, the flow-regime criteria based on the volumetric fluxes of liquid and vapor may not be consistent with the two-fluid-model formulation. This can be explained as follows. From the basic definitions of variables, the void fraction can be uniquely determined from volumetric fluxes j_g and j_f and relative velocity v_r. In a two-fluid model the relative velocity is an unknown to be solved from the field equations. Therefore, the void fraction, which is the most important geometrical parameter, cannot be determined uniquely from volumetric fluxes j_g and j_f. Consequently, a flow-regime map based on j_g and j_f alone is unsuitable to the two-fluid-model formulation. This difficulty does not arise in the drift-flux model, because the constitutive relation for the relative velocity can be used to determine the void fraction. However, for a two-fluid model, a direct geometrical parameter such as the void fraction should be used in flow-regime criteria. Some efforts in this direction have already been made in this study.

Second, two-phase flows encountered under accident conditions occur almost always under transient conditions. However, more importantly, many flows should be considered as entrance flows due to complicated geometries of the reactor systems. It is well known that a flow regime in an entrance region can be quite different from that in a developed flow. However, only very limited studies have been made for a quantitative description of these effects.[50] The flow regimes, as well as the interfacial area concentration, can be very sensitive to initial conditions. In this case, phase changes, coalescences, and disintegrations of fluid particles become very important.[1,50-62] The most general method to include these effects in the two-fluid model formulation would be to introduce a transport equation for the interfacial area concentration.[1] This equation should have source terms that account for bubble or droplet expansions or collapses, coalescences, disintegrations, and interfacial instabilities. This approach is highly conplicated; however, the inclusion of this equation is expected to make the identification of two-phase-flow regimes more mechanistic.

So far, almost no analyses have been made in this direction. Furthermore, basic experimental data needed to develop this surface-area transport equation are grossly inadequate. In view of fundamental difficulties encountered in modeling entrance and transient flow regimes under reactor accident conditions, considerable efforts should be made to develop an acceptable data base in this area.

II. INTERFACIAL INTERACTION TERMS IN TWO-FLUID MODEL

A. Two-fluid Model

A three-dimensional two-fluid model has been obtained by using temporal or statistical averaging.[1] The model is expressed in terms of two sets of conservation equations governing the balance of mass, momentum, and energy in each phase. However, since the averaged fields of one phase are not independent of the other phase, the interaction terms appear in the field equations as source terms. For most practical applications, the model developed by Ishii[1] can be simplified to the following forms:

Continuity Equation

$$\frac{\partial \alpha_k \rho_k}{\partial t} + \nabla \cdot \left(\alpha_k \rho_k \vec{v}_k\right) = \Gamma_k. \tag{1}$$

Momentum Equation

$$\frac{\partial \alpha_k \rho_k \vec{v}_k}{\partial t} + \nabla \cdot \left(\alpha_k \rho_k \vec{v}_k \vec{v}_k\right) = -\alpha_k \nabla p_k + \nabla \cdot \alpha_k \left(\bar{\bar{\tau}}_k + \tau_k^t\right)$$

$$+ \alpha_k \rho_k \vec{g} + \vec{v}_{ki} \Gamma_k + \vec{M}_{ik} - \nabla \alpha_k \cdot \tau_i. \tag{2}$$

Enthalpy Energy Equation

$$\frac{\partial \alpha_k \rho_k H_k}{\partial t} + \nabla \cdot (\alpha_k \rho_k H_k \vec{v}_k) = -\nabla \cdot \alpha_k (\bar{\bar{q}}_k + q_k^t) + \alpha_k \frac{D_k}{Dt} P_k$$

$$+ H_{ki} \Gamma_k + \frac{q''_{ki}}{L_s} + \Phi_k. \tag{3}$$

Here Γ_k, $\vec{M}_{ik}$, τ_i, q''_{ki}, and Φ_k are the mass generation, generalized interfacial drag, interfacial shear stress, interfacial heat flux, and dissipation, respectively. The subscript k denotes k phase, and i stands for the value at the interface. L_s denotes the length scale at the interface, and $1/L_s$ has the physical meaning of the interfacial area per unit volume.[1,63] Thus,

$$\frac{1}{L_s} = a_i = \frac{\text{Interfacial Area}}{\text{Mixture Volume}}. \tag{4}$$

Note that the corresponding subchannel model has been obtained from area averaging.[6]

B. Interfacial Transfer Terms

The above field equations indicate that several interfacial transfer terms appear on the right-hand sides of the equations. Since these interfacial transfer terms also should obey the balance laws at the interface, interfacial transfer conditions could be obtained from an average of the local jump conditions.[1] They are given by

$$\left.\begin{aligned} &\sum_k \Gamma_k = 0; \\ &\sum_k \vec{M}_{ik} = 0; \\ &\sum_k \left(\Gamma_k H_{ki} + q''_{ki}/L_s\right) = 0. \end{aligned}\right\} \tag{5}$$

Therefore, constitutive equations for $\vec{M}_{ik}$, q''_{1i}/L_s, and q''_{2i}/L_s are necessary for the interfacial transfer terms. The enthalpy interfacial transfer condition indicates that specifying the heat flux at the interface for both phases is equivalent to the constitutive relation for Γ_k if the mechanical-energy transfer terms can be neglected.[1] This aspect greatly simplifies the development of the constitutive relations for interfacial transfer terms.

By neglecting the lift force due to the rotations of particles and the diffusion force due to the concentration gradient, we may model the generalized drag force for a dispersed phase by a simple form[13-16] such as

$$\vec{M}_{id} = \alpha_d \vec{F}_D/B_d + \alpha_d \vec{F}_v/B_d + \frac{9}{2}\frac{\alpha_d}{r_d}\sqrt{\frac{\rho_c \mu_m}{\pi}} \int_t \frac{D_d}{D\xi}\left(\vec{v}_c - \vec{v}_d\right)\frac{d\xi}{\sqrt{t-\xi}}, \tag{6}$$

where $\vec{F}_D$, B_d, $\vec{F}_v$, and μ_m are the standard drag force, volume of a typical particle, virtual mass force, and mixture viscosity, respectively. The last term is the Basset force. The standard drag force acting on the particle under steady-state conditions can be given in terms of the drag coefficient C_D based on the relative velocity as

$$\vec{F}_D = -\frac{1}{2} C_D \rho_c \vec{v}_r |v_r| A_d, \tag{7}$$

where A_d is the projected area of a typical particle and $\vec{v}_r$ is the relative velocity given by $\vec{v}_r = \vec{v}_d - \vec{v}_c$. Hence, the portion of $\vec{M}_{id}$ represented by the drag force becomes

$$\alpha_d \vec{F}_D/B_d = -\left(\alpha_d \frac{A_d}{B_d}\right)\frac{C_D}{2}\rho_c \vec{v}_r |v_r|. \tag{8}$$

Now for a dispersed flow system, several important length scales[64] can be defined as follows.

$$\text{Sauter mean radius:} \quad r_{sm} \equiv \frac{3B_d}{A_i}. \tag{9}$$

$$\text{Drag radius:} \quad r_D \equiv \frac{3B_d}{4A_d}. \tag{10}$$

$$\text{Equivalent radius:} \quad r_v \equiv \left(\frac{3}{4\pi} B_d\right)^{1/3}. \tag{11}$$

$$\text{Surface radius:} \quad r_s \equiv \left(\frac{A_i}{4\pi}\right)^{1/2}. \tag{12}$$

Here A_i is the surface area of a typical particle. For spherical particles, the above-defined radii are all equivalent. The number density N_d of a dispersed phase is given by

$$N_d = \frac{\alpha_d}{B_d} \tag{13}$$

and the interfacial area concentration a_i by

$$a_i = N_d A_i. \tag{14}$$

Using the above definitions, we can express the area concentration in a number of forms. For example,

$$a_i = \frac{3\alpha_d}{r_{sm}} = \frac{3\alpha_d}{r_v}\left(\frac{r_s}{r_v}\right)^2 = \frac{3\alpha_d}{r_D}\left(\frac{r_D}{r_{sm}}\right). \tag{15}$$

Therefore, from Eqs. 8, 10, and 15, the drag term becomes

$$\alpha_d \vec{F}_D / B_d = -a_i\left[\frac{C_D}{4}\left(\frac{r_{sm}}{r_D}\right)\frac{\rho_c \vec{v}_r |v_r|}{2}\right]. \tag{16}$$

This indicates that the drag force per unit volume of mixture is proportional to the interfacial area concentration and drag coefficient. The ratio of the Sauter mean radius to the drag radius appears on the right-hand side of Eq. 16 as a shape factor.

By introducing the mean mass transfer per unit area defined by

$$\Gamma_k \equiv a_i \overline{m_k}, \tag{17}$$

we can rewrite the interfacial energy-transfer term in Eq. 3 as

$$\Gamma_k H_{ki} + \frac{q''_{ki}}{L_s} = a_i\left(\overline{m_k} H_{ki} + q''_{ki}\right). \tag{18}$$

The heat flux at the interface should be modeled using the driving force or the potential for an energy transfer. Thus,

$$q''_{ki} = h_{ki}\left(T_i - T_k\right), \tag{19}$$

where T_i and T_k are the interfacial and bulk temperatures based on the mean enthalpy. In view of Eqs. 16-18, the importance of the interfacial area, a_i, in developing constitutive relations for these terms is evident. The interfacial transfer terms are now expressed as a product of the interfacial area and the driving force. It is essential to make a conceptual distinction between the effects of these two parameters. The interfacial transfer of mass, momentum, and energy increases with an interfacial-area concentration toward the mechanical and thermal equilibrium.

III. INTERFACIAL MOMENTUM TRANSFER

A. Drag Coefficient

The drag correlation for a single-particle system depends not only on the flow regimes but also on the nature of the particles, i.e., solid particle, drop, or bubble. Therefore, for a multiparticle system, these differences are also expected to play central roles in determining the drag correlation. In the present study, the multiparticle drag correlation is developed in parallel with the single-particle system by considering the following flow regimes:

Solid-particle system
- Viscous regime
- Newton's regime

Fluid-particle system
- Viscous regime (Undistorted-particle regime)
- Distorted-particle regime
- Churn-turbulent-flow regime
- Slug-flow regime

In the viscous regime, distortions of fluid particles are negligible. Therefore, for this regime, solid- and fluid-particle systems are considered together. The other flow regimes are analyzed separately because of significant differences in the flow around the particles and the motions of the interfaces. A detailed analysis of the two-phase drag coefficient is reported in Ishii and Chawla.[16]

Table I summarizes the present drag coefficient in various flow regimes. Their dependence on the Reynolds number and particle concentration is shown in Figs.1-6. Since these correlations are obtained from the assumed similarity hypothesis, their validity should be tested against experimental data. In a multiparticle system, a drag force cannot be measured directly under normal conditions. Therefore considerable care should be taken in these comparisons.

The comparison of the theoretical predictions to over 1000 experimental data in terms of the relative velocity indicated that satisfactory agreement could be obtained at wide ranges of the particle concentration and Reynolds number. For spherical-solid-particle systems, the data from the Stokes regime up to the Newton's regime within the concentration range of 0-0.55 were examined. For fluid-particle systems, the distorted-particle and churn-turbulent regimes were extensively studied because of their practical importance. The success of the present correlation at up to the highest concentration range for spherical-solid-particle systems was accomplished by introducing the maximum

TABLE I. Local Drag Coefficients in Multiparticle System

	Fluid Particle System			Solid Particle System
	Bubble in Liquid	Drop in Liquid	Drop in Gas	
Viscosity Model	$\frac{\mu_m}{\mu_c} = \left(1 - \frac{\alpha_d}{\alpha_{dm}}\right)^{-2.5\alpha_{dm}\mu^*}$, $\mu^* \equiv \frac{\mu_d + 0.4\mu_c}{\mu_d + \mu_c}$			
Max. Packing α_{dm}	~ 1	~ 1	$0.62 \sim 1$	~ 0.62
μ^*	0.4	~ 0.7	1	1
$\frac{\mu_m}{\mu_c}$	$(1-\alpha_d)^{-1}$	$(1-\alpha_d)^{-1.75}$	$\sim(1-\alpha_d)^{-2.5}$	$\left(1 - \frac{\alpha_d}{0.62}\right)^{-1.55}$
Stokes Regime C_D	$C_D = 24/N_{Re}$ where $N_{Re} = 2r_d\rho_c v_r/\mu_m$			
Viscous Regime C_D	$C_D = 24\ (1 + 0.1\ N_{Re}^{0.75})/N_{Re}$			
Newton's Regime C_D	—			$C_D = 0.45\left\{\frac{1 + 17.67[f(\alpha_d)]^{6/7}}{18.67\ f(\alpha_d)}\right\}^2$ where $f(\alpha_d) = \sqrt{1-\alpha_d}\left(\frac{\mu_c}{\mu_m}\right)$
Distorted Particle Regime C_D	$C_D = \frac{4}{3} r_d \sqrt{\frac{g\Delta\rho}{\sigma}} \left\{\frac{1 + 17.67[f(\alpha_d)]^{6/7}}{18.67\ f(\alpha_d)}\right\}^2$ $f(\alpha_d) = (1-\alpha_d)^{1.5}$ $(1-\alpha_d)^{2.25}$ $(1-\alpha_d)^3$			
Churn-Turbulent Flow Regime C_D	$C_D = \frac{8}{3}(1-\alpha_d)^2$			
Slug Flow C_D	$C_D = 9.8\ (1-\alpha_d)^3$			

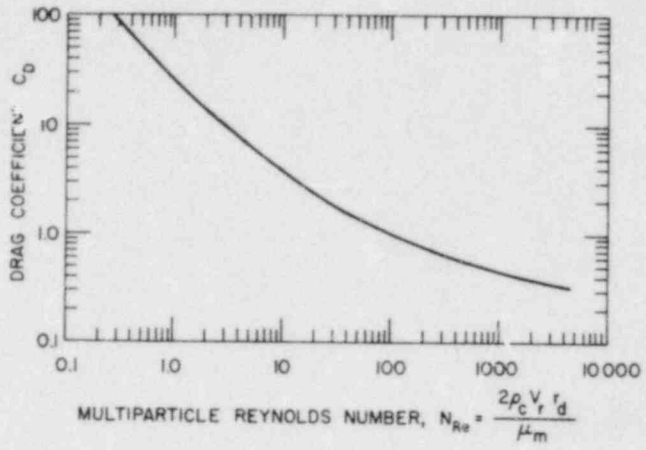

Fig. 1

Drag Coefficient in Viscous Regime.
ANL Neg. No. 900-79-614.

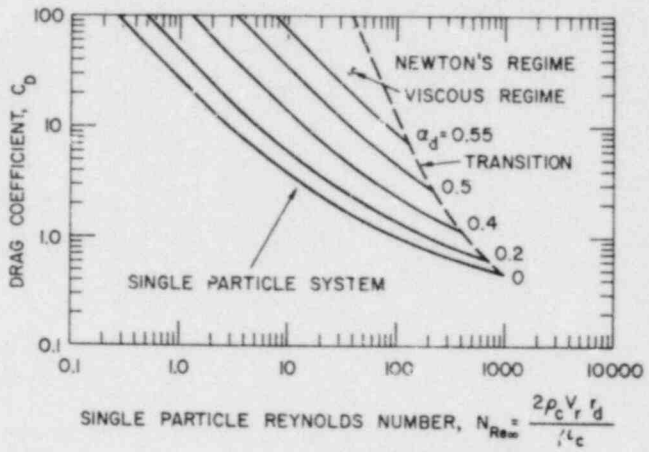

Fig. 2

Effect of Concentration on Drag Coefficient in Viscous Regime.
ANL Neg. No. 900-79-613 Rev.

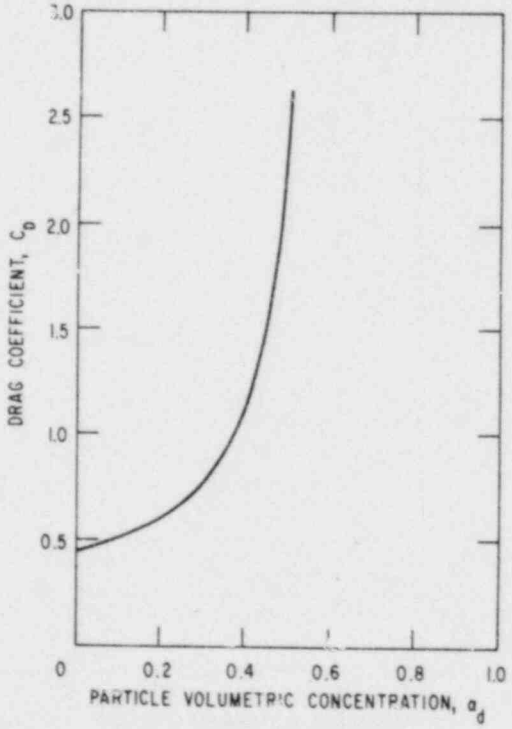

Fig. 3

Drag Coefficient for Multi-particle Newton's Regime.
ANL Neg. No. 900-79-617.

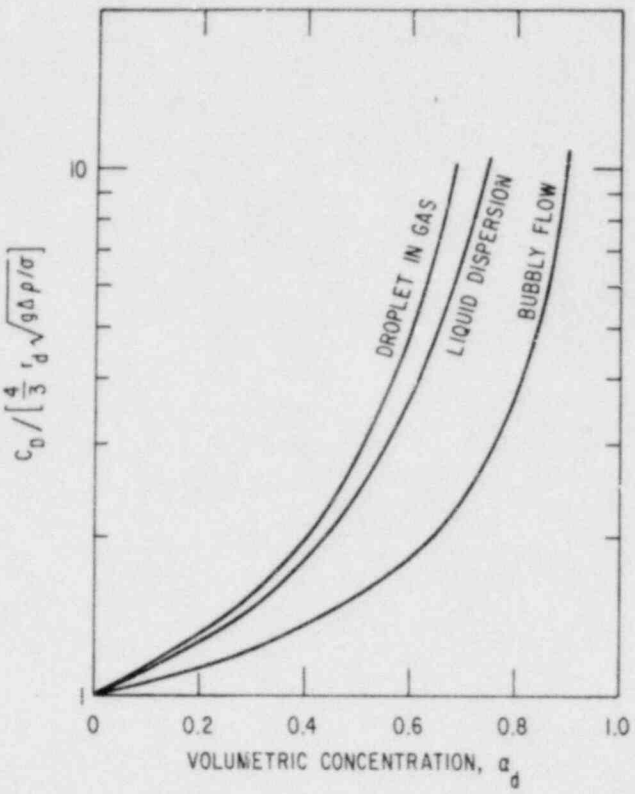

Fig. 4. Drag Coefficient in Distorted-particle Regime. ANL Neg. No. 900-79-616.

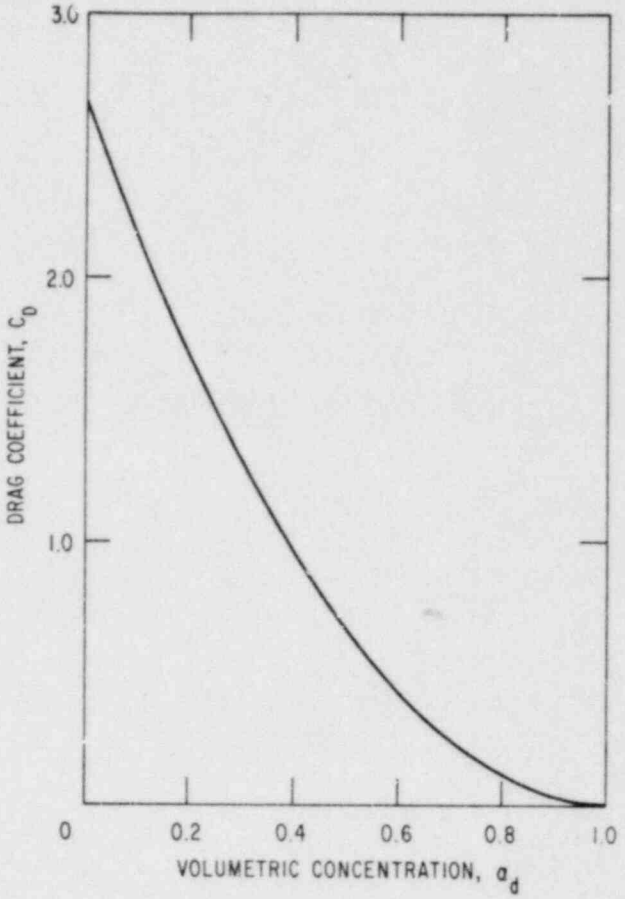

Fig. 5. Drag Coefficient for Churn-turbulent Flow. ANL Neg. No. 900-79-619.

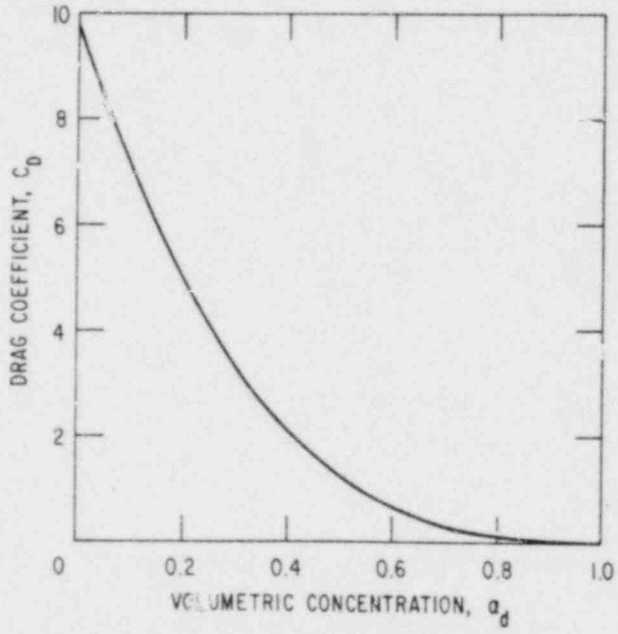

Fig. 6

Drag Coefficient for Slug Flow. ANL Neg. No. 900-79-618.

packing in the mixture-viscosity relation. This was a definite improvement over the existing correlations. Note also that the present model was sufficient up to the foam or dense-packing regime with the concentration ranging from 0.5 to 0.95 for both bubbly and droplet flows. These comparisons indicated that the postulated drag-similarity law based on the mixture-viscosity concept was appropriate. Therefore, the drag law governing the motions of bubbles, drops, and particles in various dispersed two-phase flows can be explained by a unified and consistent model developed under the present study.

The present correlation for the drag coefficient for multiparticle systems has been developed from the steady-state and adiabatic formulation. It was postulated that the transient effect on the momentum-exchange term could be taken into account by an essentially linear constitutive relations. Therefore, it was indirectly assumed that the standard drag coefficient developed in the analysis could also be used under transient conditions. The additional interfacial forces due to the inertia effect and development of a boundary layer in transient flow are considered separately.

The phase change at the particle surface contributes to the interfacial momentum transfer in two different ways. There is a direct effect of momentum carried by the mass undergoing phase change, as can be seen from the momentum equation. Changing particle size or shape due to phase change and modifying the boundary layer around the particles by additional mass flux normal to the surface may affect the standard drag coefficient. However, the effects of heat-transfer and phase changes are considered as secondary in the present analysis. These effects appear only indirectly through the local variables such as the void fraction, particle sizes, and component velocities. To assess the significance of the phase-change effect on the drag coefficient apparently requires further experimental and analytical studies.

B. Transient Forces

The generalized drag force for a dispersed two-phase flow has been modeled as a linear combination of three forces in Eq. 6. The significance of the various terms in the equation is as follows: The term on the left-hand side represents the combined interfacial drag forces acting on the dispersed phase. The first term on the right-hand side is the skin and form drag under the steady-state condition. The second term is the force required to accelerate the apparent mass of the surrounding phase when the relative velocity changes. The third term, known as the Basset force, is the effect of the acceleration on the viscous drag and the boundary-layer development.

The forms of these two transient terms have not been firmly established. Because of their importance under transient conditions and for numerical-stability problems, further research in this area was required. Zuber[13] studied the effect of the concentration on the virtual mass force and obtained

$$\alpha_d \vec{F}_v / B_d = -\frac{1}{2}\alpha_d \frac{1 + 2\alpha_d}{1 - \alpha_d} \rho_c \frac{D_d}{Dt}(\vec{v}_d - \vec{v}_c). \tag{20}$$

Lahey et al.[11] studied a necessary condition for the constitutive equation for the virtual mass term. From the requirement of the frame indifference of the constitutive equation, they determined that the virtual mass force $\vec{F}_v$ should satisfy

$$\vec{F}_v \propto \left[\frac{D_d \vec{v}_d}{Dt} - \frac{D_c \vec{v}_c}{Dt} + (1 - \lambda)\vec{v}_r \cdot \nabla v_r\right]. \tag{21}$$

In view of Zuber's study[13] on the effect of concentration and the above frame-indifference condition, a new form for $\vec{F}_v$ is proposed here. Due to the acceleration of the particles relative to the fluid, the acceleration drag arises. This should be proportional to the induced mass $\rho_c B_d^*$ and the frame-indifferent relative-acceleration vector. Hence,

$$\vec{F}_v = -\rho_c B_d^* \left[\frac{D_d \vec{v}_d}{Dt} - \frac{D_c \vec{v}_c}{Dt} + (1 - \lambda)\vec{v}_r \cdot \nabla \vec{v}_r\right]. \tag{22}$$

The value of induced mass $\rho_c B_d^*$ for a single particle in an infinite medium can be obtained from potential theory. Hence, the limiting value of $\vec{F}_v$ at $\alpha_d \to 0$ for a spherical particle is

$$\lim_{\alpha_d \to 0} \vec{F}_v = -\frac{1}{2}\rho_c B_d \frac{D_d(\vec{v}_d - \vec{v}_c)}{Dt}. \tag{23}$$

From this limit, it can be shown that

$$\lim_{\alpha_d \to 0} B_d^* = \frac{1}{2} B_d \tag{24}$$

and

$$\lim_{\alpha_d \to 0} \lambda = 2. \tag{25}$$

If λ is constant in Eq. 22, the value of λ should be 2.

The effect of the concentration on B_d^* can be taken into account by the method used by Zuber.[13] Thus, from the solution for the induced mass for a sphere moving within an outer sphere,[65] B_d^* may be approximated by

$$\rho_c B_d^* \doteq \frac{1}{2}\rho_c B_d \frac{B_c + 2B_d}{B_c - B_d}, \tag{26}$$

where B_c is the volume of the outer sphere representing the total mixture volume. Hence, by definition,

$$\alpha_d \equiv \frac{B_d}{B_c}. \tag{27}$$

Substituting Eq. 27 into Eq. 26, we obtain

$$B_d^* = \frac{1}{2} B_d \frac{1 + 2\alpha_d}{1 - \alpha_d}. \tag{28}$$

Under the assumption of λ = constant, the constitutive equation for the virtual mass force is obtained from Eqs. 22 and 28 as

$$\alpha_d \vec{F}_v / B_d = -\frac{1}{2} \alpha_d \frac{1 + 2\alpha_d}{1 - \alpha_d} \rho_c \left(\frac{D_d \vec{v}_r}{Dt} - \vec{v}_r \cdot \nabla \vec{v}_c \right). \tag{29}$$

The above equation indicates that the virtual mass force $\vec{F}_v$ per particle increases considerably with increasing particle concentration. This relation implies that the effect of concentration on dynamic coupling can be scaled by a factor of $(1 + 2\alpha_d)/(1 - \alpha_d)$. Mokeyev[66] used an electrohydrodynamic analog method to determine the velocity potential through an electric field potential and obtained an empirical function

$$B_d^*/B_d = 0.5 + 2.1\alpha_d.$$

The theoretical result of Eq. 28 compared favorably with this correlation.

A correlation for the virtual mass force in a slug flow can be developed from a simple potential flow analysis using a Bernoulli equation. First, a cylindrical bubble of length L_b with diameter D_b in a tube of diameter D is considered, as shown in Fig. 7a. Then the void fraction in a slug-bubble

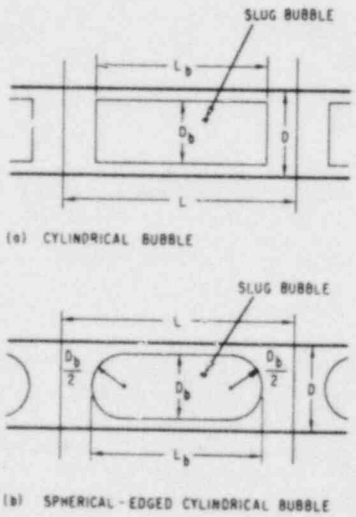

Fig. 7

Slug-flow Model for Virtual-mass-force Analysis

section is given by

$$\alpha_b = \frac{D_b^2}{D^2}, \tag{30}$$

and the average overall void fraction α_d by

$$\alpha_d = \frac{L_b}{L}\,\alpha_b, \tag{31}$$

where L is the pitch. Now, let the continuous phase accelerate with respect to a bubble. This will generate a pressure force acting on a bubble due to the acceleration along the film section. From a simple one-dimensional analysis, this force can be found as

$$F_v = -\frac{\pi}{4} D_b^2 L_b \frac{\rho_c}{1-\alpha_b} \frac{\partial v_r}{\partial t}. \tag{32}$$

However, the volume of a bubble is given by $B_d = (\pi/4)D_b^2 L_b$. Thus, the virtual mass force per unit volume becomes

$$\alpha_d \vec{F}_v / B_d = -\alpha_d \frac{\rho_c}{1-\alpha_b} \frac{\partial \vec{v}_r}{\partial t} \simeq -5\alpha_d \rho_c \frac{\partial \vec{v}_r}{\partial t}. \tag{33}$$

Here the second form is obtained by approximating the void fraction in the slug-bubble section by $\alpha_b \simeq 0.8$.

The second case considered is a train of spherical-edged cylindrical bubbles, as shown in Fig. 7.b. Application of the Bernoulli equation

$$\frac{\partial \Phi}{\partial t} + \int \frac{dp}{\rho} + \Omega + \frac{v^2}{2} = \text{const.} \tag{34}$$

to this geometry under a relative acceleration yields

$$\alpha_d \vec{F}_v / B_d = -\left[\alpha_d + \frac{3}{2}\left(\frac{\alpha_d}{\alpha_b} - \frac{L_b - D_b}{L}\right)\left(\frac{\alpha_b}{3} - 1 + \sqrt{\frac{1-\alpha_b}{\alpha_b}}\ \arctan\sqrt{\frac{\alpha_b}{1-\alpha_b}}\right)\right] \frac{\rho_c}{1-\alpha_b} \frac{\partial \vec{v}_r}{\partial t}. \tag{35}$$

By using an approximation $\alpha_b \simeq 0.8$, the virtual mass force becomes

$$\alpha_d \vec{F}_v / B_d = -5\left(0.66\alpha_d + 0.27\,\frac{L_b - D_b}{L}\right)\rho_c \frac{\partial \vec{v}_r}{\partial t}. \tag{36}$$

For a limiting case of a train of spherical bubbles, $L_b = D_b$, the above equation reduces to

$$\alpha_d \vec{F}_v / B_d = -3.3\alpha_d \rho_c \frac{\partial \vec{v}_r}{\partial t}. \tag{37}$$

On the other hand, if $L_b >> D_b$, L_b/L can be approximated by α_d/α_b. Thus for long slug bubbles, Eq. 36 essentially converges to the simple solution given by Eq. 33. The virtual mass force for a slug flow given by Eq. 36 is expressed in terms of the relative acceleration in the absence of a large convective acceleration. However, if the convective acceleration cannot be neglected, a special convective derivative in the form of Eq. 22 may be more appropriate. Thus, for a general case,

$$\alpha_d \vec{F}_v / B_d = -5\left(0.66\alpha_d + 0.27 \frac{L_b - D_b}{L}\right)\rho_c \left(\frac{D_d \vec{v}_r}{Dt} - \vec{v}_r \cdot \nabla \vec{v}_c\right). \tag{38}$$

Now the solutions for a dispersed flow, Eq. 29, and slug flow, Eq. 38, can be examined by introducing an induced mass coefficient C_M defined by

$$\alpha_d \vec{F}_v / B_d = -C_M \rho_c \left(\frac{D_d \vec{v}_r}{Dt} - \vec{v}_r \cdot \nabla \vec{v}_c\right), \tag{39}$$

where

$$C_M = \begin{cases} \frac{1}{2}\alpha_d \frac{1 + 2\alpha_d}{1 - \alpha_d} & \text{(Bubbly flow)} \\ 5\alpha_d \left(0.34 \frac{1 - D_b/L_b}{1 - D_b/3L_b}\right). & \text{(Slug flow)} \end{cases} \tag{40}$$

A plot of C_M against α_d is shown in Fig. 8. The virtual mass force increases with an increasing void fraction of a dispersed phase, due to stronger

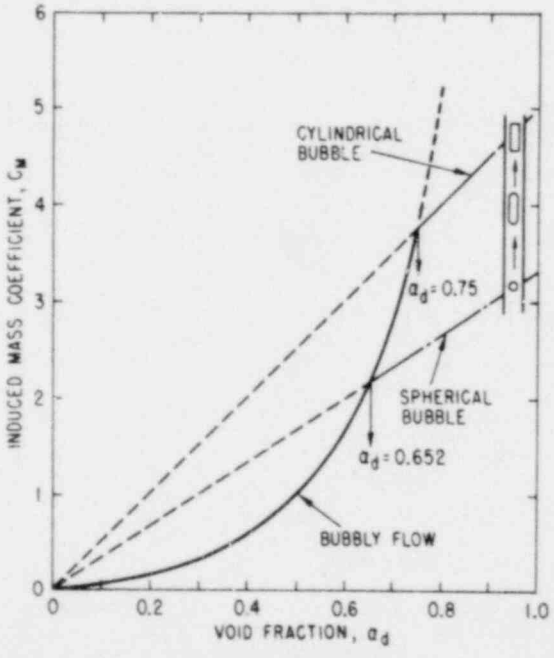

Fig. 8

Virtual Mass Coefficient for Dispersed and Slug-flow Regimes

coupling between two phases. The intersection of the above two solutions occurs at the void fraction between 0.66 and 0.75. For a lower void fraction, the virtual mass force for a bubbly flow is smaller than that for a slug flow. This implies that the vapor phase has less resistance to an acceleration in a bubbly-flow configuration than in a slug-flow configuration if $\alpha_d < 0.66$. This may also suggest that an accelerating slug flow has a tendency to disintegrate into a bubbly flow when $\alpha_d < 0.66$. On the other hand, for $\alpha_d > 0.66$, a slug flow should be quite stable, even under a transient condition.

Due to a similarity in flow geometries, the virtual mass force for a churn-turbulent flow may be approximated by the solution for a slug flow given by Eq. 36. In a liquid dispersed flow, the virtual mass force becomes considerably smaller than that in a vapor dispersed flow. This decrease is caused by a change in the continuous phase density to be used in Eq. 29. By changing the continuous phase from liquid to vapor, the virtual mass force for a droplet flow becomes insignificant.

IV. EXPERIMENTAL OBSERVATION ON INTERFACIAL AREA

A. Experimental Method

A number of experimental studies[18-38] on interfacial areas have been published in chemical-engineering fields in the past 15 years. Most of these experiments used a chemical-absorption technique[40] based on a pseudo-first-order chemical reaction. These experiments were performed by using two fluids such as air and water. Then some reacting gas such as CO_2 is added to air, and reacting liquid such as NaOH to water. If the reaction is a fast, irreversible, pseudo-first-order chemical reaction, the average interfacial area between two sampling points can be measured by applying the surface-renewal theory of Danckwerts. Sharma and Danckwerts[40] have given a good review of this method in terms of chemical combinations and geometries of systems.

Other important techniques for measuring interfacial areas are the light-attenuation[41] and photography[21] methods, which require a flow channel with transparent walls. The advantages and shortcomings of various methods are discussed by Landau et al.[42] The chemical method[19,20,22-30] is the most widely used technique and probably the most reliable one. The value of the interfacial area can be obtained by a simple measurement. However, it can be applied only to a case without phase changes, and experimentation is time-consuming. The light-attenuation method[43] is simple, and cross-sectional area-averaged measurements at various axial locations are possible. However, the measurement depends on flow regimes and is applicable only when interferences due to multiple and forward light scattering are negligibly small. The photography method[21,30] involves very time-consuming data analyses. One should measure particle sizes in detail from photographs. This may require up to 24 hours of tedious work per picture. Furthermore, the method is good only at relatively low concentration of a dispersed phase. The light-attenuation and photography methods are applicable to a flow with phase changes; however, bounding walls and fluid should be transparent.

In principle, a local measurement of interfacial areas is possible using a three-point probe as suggested by Delhaye. Each point identifies a phase surrounding that point. For example, optical probes, resistive probes, or micro-thermocouples can be used for this purpose. Three probes should be located very close to each other. The distance between these three points must be smaller than bubble or droplet sizes. Because of these requirements, this method has not been put into practice. Three existing methods also have a number of limitations as explained above. Although some experimental data for interfacial areas are available, the ranges of experimental conditions are very limited.

B. Evaluation of Existing Data

Among available experimental data,[18-38] only about one-third of them were for straight tubes or channels.[19-26] These important data for straight tubes are summarized in Table II. Watson et al.,[19] Kasturi and Stepanek,[22] and Shilimkan and Stepanek[20] used an air-water system with the chemical-absorption technique for vertical cocurrent upflows. The flow regimes observed in these experiments were mainly slug, churn-turbulent, or annular flows. The tube, diameters used were 0.6 cm,[22] 1-2 cm,[20] and 2.54 cm.[19]

The liquid flow rates were relatively low, i.e., 3-50 cm/s. However, a wide range of gas flow rates was covered, from 0.3 to 30 m/s. The observed interfacial area concentrations are plotted against the gas volumetric flux with the liquid flux as a parameter in Figs. 9-13. The range of values for interfacial area reported in these experiments was 1-10 cm^2/cm^3. In general, the interfacial area increased with an increase in the gas flux at relatively low gas fluxes corresponding to the slug or churn-turbulent flow. This may indicate the existence of a large number of small bubbles. These bubbles should have been produced by increased shearing actions within the liquid due to turbulent motions.

Besides this general trend, most of the data, except those of Kasturi and Stepanek,[22] showed the existence of local maxima of the interfacial area, as shown in Figs. 10-13. The most clearly indicated maximum occurred at the gas volumetric flux in the vicinity of 2 m/s. This may be attributed to the increased coalescences of small bubbles into larger ones and also among larger bubbles. These coalescences characterize the transition to the churn-turbulent-flow regime. A possibility of another local maximum of the interfacial area can be seen in Figs. 11 and 12. This maximum occurred only for limited cases at much smaller gas flux than the first one. Figure 12 indicates the gas volumetric flux of 0.4 m/s at the maximum. This point may correspond to the bubbly-flow to slug-flow transition. However, there are no firm experimental observations or data to back up this speculation.

The experimental data points in Figs. 9-13 are distinguished by symbols denoting flow regimes. Note that these flow regimes are predicted by the present model discussed in Sec. VI. For most data the information on the flow regime has been insufficiently documented, except the data of Watson et al.[19] The above discussed experimental data fall into the slug, churn-turbulent, and annular-flow regime. The important regimes of a bubbly flow and the transition regime between bubbly and slug flows are completely missing from these experiments.

The effects of the tube diameter on the interfacial area have been studied by plotting these data on an a_i-j_g plane with fixed liquid flow rates and the tube diameter as a parameter in Figs. 14-16. There are considerable differences in interfacial areas among the data taken for tubes of not much different sizes, i.e., 0.6, 1, 1.5, 2, and 2.54 cm. However, the effects of the diameter

TABLE II. Experimental Data on Interfacial Area for Simple Geometry

Authors	Geometry (cm)	Fluid	Flow Rate	Flow Regime	Remarks
Watson et al.	2.54Φ × 454	Air - Water	j_g = 1 ∿ 8 m/s j_f = 3 ∿ 50 cm/s	slug, churn (Vertical up)	a_i = 1 ∿ 7 (cm^2/cm^3) 50 data
Kasturi Stepanek	0.6Φ × 152	Air - Water	j_g = 0.6 ∿ 12 m/s j_f = 7 ∿ 51 cm/s	slug, churn, annular (Vertical up)	a_i = 1 ∿ 10 40 data
Shilimkan Stepanek	1Φ × 152 1.5Φ 2.0Φ	Air - Water	j_g = 0.3 ∿ 30 m/s j_f = 5 ∿ 35 cm/s	slug, churn, annular (Vertical up)	a_i = 1 ∿ 5 150 data
Burgess Calderbank	Sieve Tray 24 × 30 × 15 (W × D × H)	Air - Water	j_g = 0.3 ∿ 0.9 m/s j_f = 1.4 ∿ 3 cm/s	slug, churn (Semi-Vertical)	a_i = 1 ∿ 3 10 data
Akita Yoshida	7.7 × 7.7 × 250 15 × 15 30 × 30	Air - Water - Glycol - Methanol	j_g < 0.04 m/s j_f ≈ 0	bubbly (Vertical up)	a_i = 0.02 ∿ 0.7 60 data
Sharma Mashelkar	6.6Φ 38.5Φ	Air - Water	j_g = 0.15 ∿ 0.4 m/s j_f ≈ 0	bubbly (Vertical up)	a_i = 1.8 ∿ 3.2 20 data
Linsted et al.	3.2Φ × 180	Air - Water	j_g = 9 ∿ 22 m/s j_f = 0.1 ∿ 15 cm/s	annular (Vertical up)	no direct data on a_i data on
Shah Sharma	0.8Φ × 150 1.2Φ	O_2 - Water - Glycol	j_g = 0.05 ∿ 0.44 m/s j_f = 0.15 ∿ 0.55 cm/s	bubbly, slug (Horizontal)	a_i = 0.5 ∿ 5 30 data Effect of μ,σ
Gregory Scott	1.9Φ × 720	CO_2 - Water	j_g = 1 ∿ 7 m/s j_f = 22 - 80 cm/s	bubbly, slug (Horizontal)	a_i = 0.5 ∿ 2.5 120 data
Wales	2.54 × 730	Air - Water	j_g = 18 ∿ 37 m/s j_f = 12 ∿ 62 cm/s	annular mist (Horizontal)	a_i = 3.5 ∿ 23.5 35 data

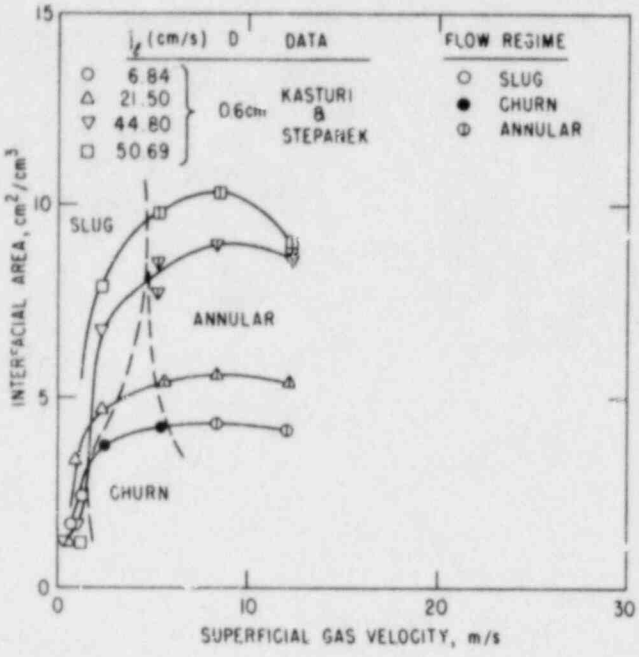

Fig. 9

Cocurrent Upward-flow Data of Kasturi and Stepanek[22] for Interfacial Area in 0.6-cm Tube

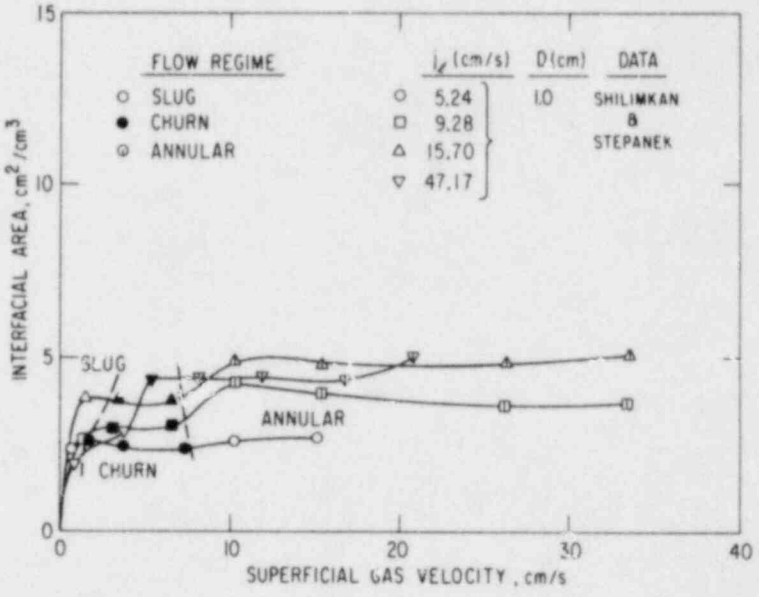

Fig. 10

Cocurrent Upward-flow Data of Shilimkan and Stepanek[26] for Interfacial Area in 1.0-cm Tube

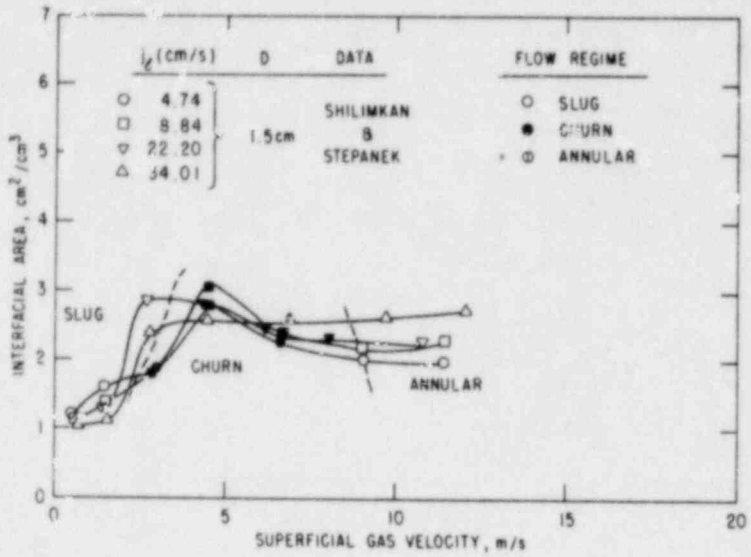

Fig. 11

Cocurrent Upward-flow Data of Shilimkan and Stepanek[20] for Interfacial Area in 1.5-cm Tube

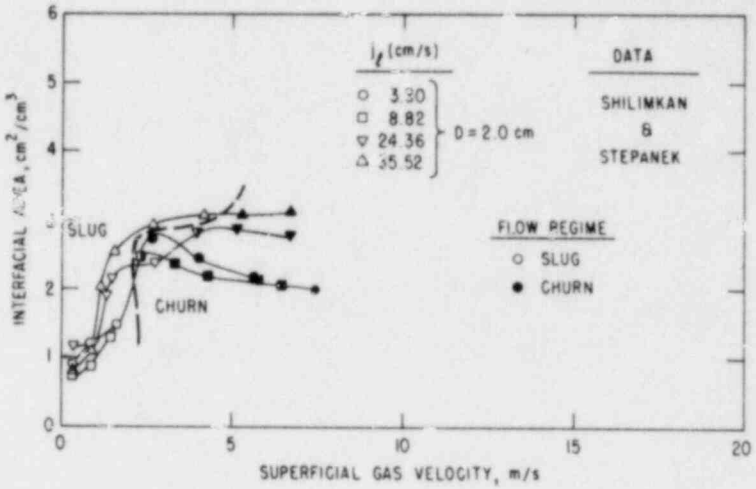

Fig. 12

Cocurrent Upward-flow Data of Shilimkan and Stepanek[20] for Interfacial Area in 2.0-cm Tube

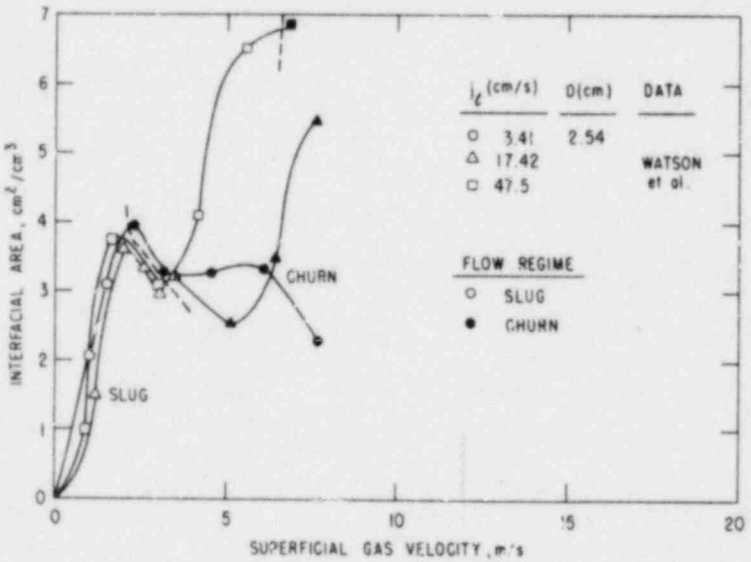

Fig. 13

Cocurrent Upward-flow Data of Watson et al.[19] for Interfacial Area in 2.54-cm Tube

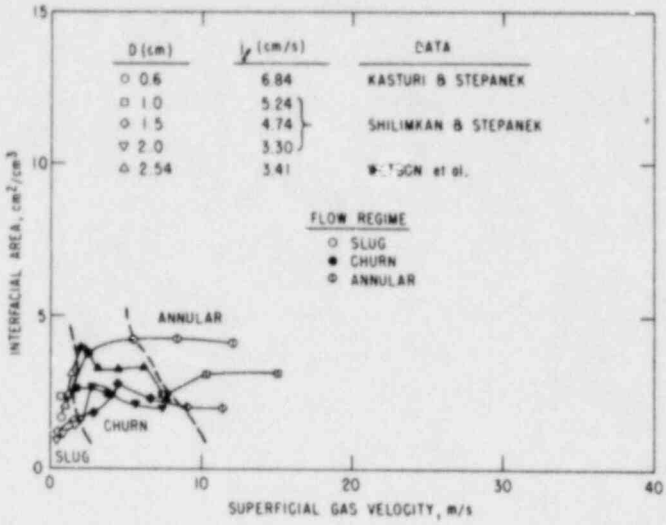

Fig. 14

Effect of Tube Diameter on Interfacial Area at Low Liquid Flow

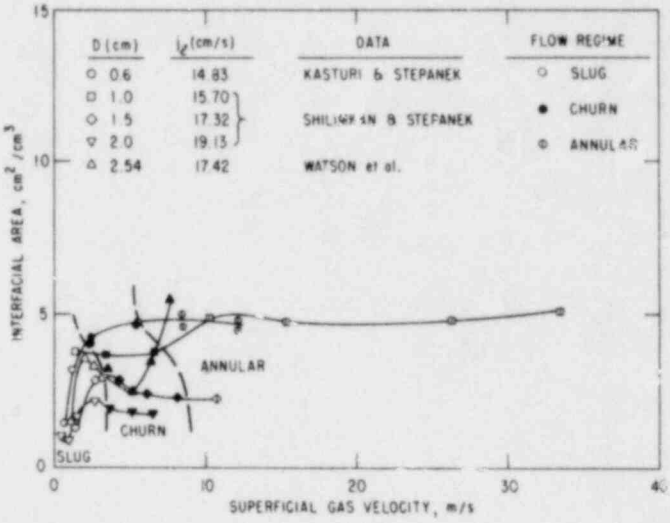

Fig. 15

Effect of Tube Diameter on Interfacial Area at Intermediate Liquid Flow

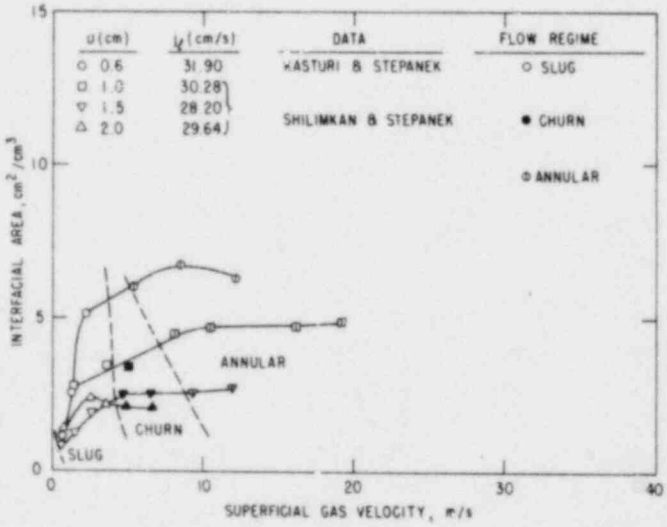

Fig. 16

Effect of Tube Diameter on Interfacial Area at Relatively High Liquid Flow

are so mixed that no general trends can be observed from these data. The data scattering among different experiments may indicate the sensitivity of the interfacial area to various experimental conditions such as inlet conditions and the existence of surface contamination. Note also that the chemical method for interface area measurements is accompanied with a standard error of at least ±10%.

Akita and Yoshida[21] used the photography method to determine bubble-size distribution and interfacial areas for bubbly flow in several square columns. The test sections were made of transparent acrylic resin and had cross sections of 7.7 x 7.7, 15 x 15, and 30 x 30 cm with a height of 250 cm. The experiments were performed at very low gas flux, $j_g < 0.042$ m/s. The range of the void fraction was $0.003 < \alpha < 0.1$, and the measured interfacial areas were within $0.021 < a_i < 0.66$ cm^2/cm^3. Relatively small interfacial areas were due to the large size of bubbles, typically 0.6 cm, and low void fractions.

Sharma and Mashelkar[18] used bubble columns of diameter from 6.6 to 38.5 cm to measure interfacial areas, as shown in Fig. 17, which indicates that the surface area increased almost linearly with the increasing gas volumetric flux. Due to the existence of many small bubbles, the values of the interfacial area can be considerably higher than that for slug flow.

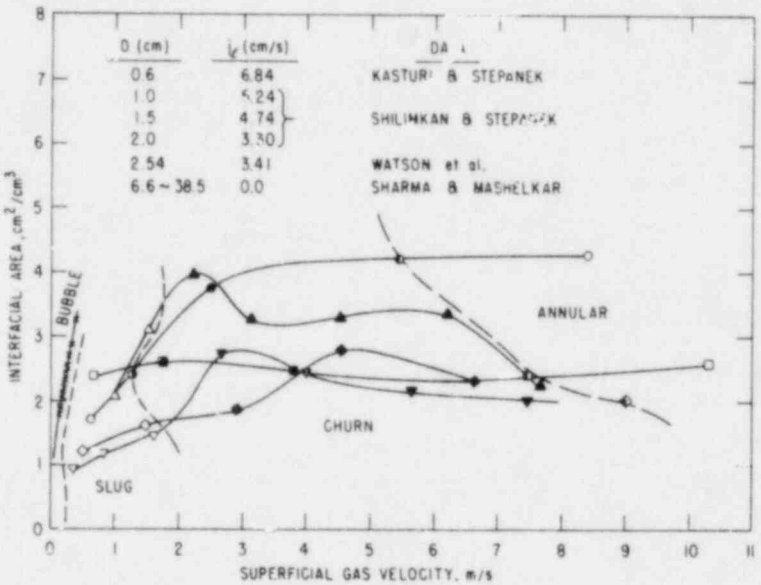

Fig. 17. Interfacial Area in Bubbly Flow in Comparison with Other Flow Regimes

Figure 18 shows the experimental ranges of the above-discussed experimental data for a vertical cocurrent flow.[19-22] The figure indicates that the ranges of available data are very limited. For example, there are no data at higher liquid flow rates beyond $j_f = 0.5$ m/s. Data for the bubbly- to slug-flow transition range are also completely missing. Most of the data cover the slug-to-churn and churn-to-annular-flow transitions. Data at very low liquid

flow and high gas flow are quite inadequate. In this range, the data of Burgess and Calderbank[30] for a sieve tray are important, although the test section is very short and the flow is three-dimensional. Apparently there are no data on interfacial areas in countercurrent and cocurrent downflows, which are important in terms of nuclear-reactor applications.

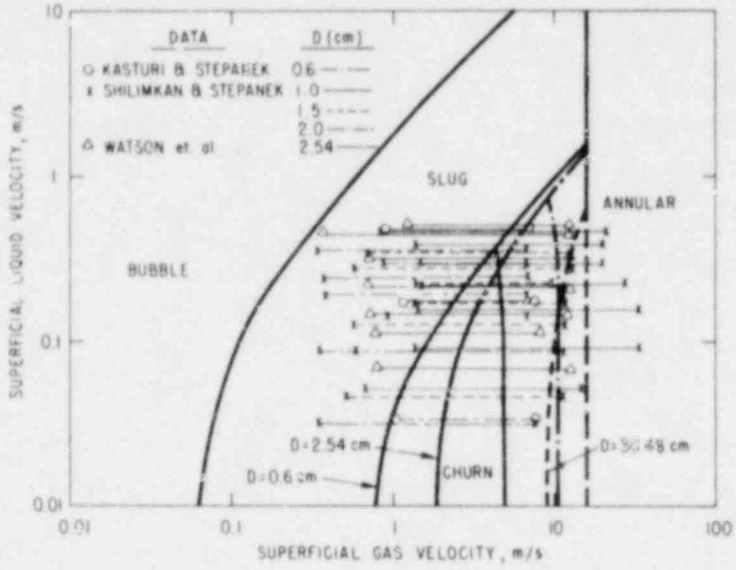

Fig. 18

Ranges of Data for Interfacial Area in Cocurrent Upward Flow

For a horizontal flow, there are three widely different experimental data of Shah and Sharma,[25] Gregory and Scott,[24] and Wales,[26] as seen in Table II. The experiment of Shah and Sharma was performed at very low gas fluxes; however, the corresponding liquid fluxes were relatively high. The observed interfacial areas were between 0.5 and 4 cm^2/cm^3. These high values indicate that the flow should have been either in the bubbly or bubbly-to-slug transition regime. The very steep rise of a_i with respect to increases in j_g is in interesting contrast with the data of Gregory and Scott,[24] as shown in Fig. 19. The latter data show that, at low gas fluxes, the value of a_i is in the order of 0.5-1 cm^2/cm^3. The local maximum of the interfacial area concentration occurred at $j_g \approx 1.5$ m/s, which roughly corresponds to the transition between the elongated-bubble regime and the slug-flow regime. In the slug-flow regime, the interfacial area concentration increases gradually with increases in the gas flow rate up to 2 cm^2/cm^3.

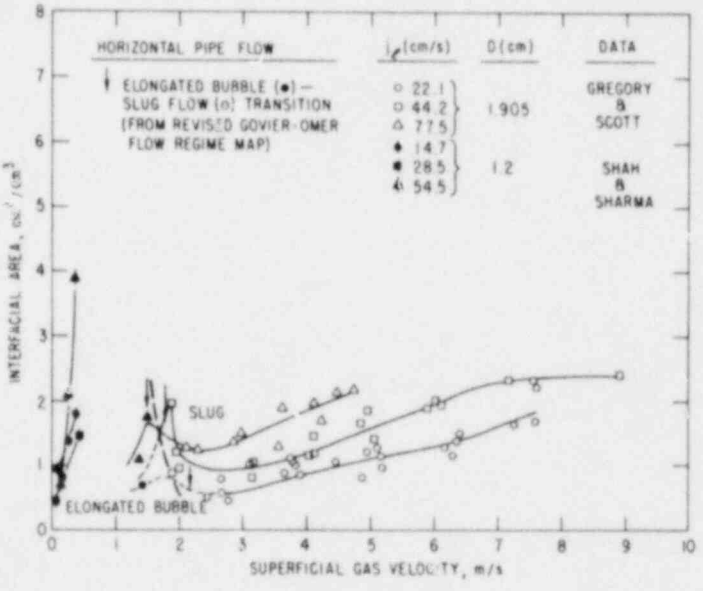

Fig. 19. Experimental Data of Interfacial Area at Relatively Low Gas Volumetric Flux

The data of Wales were taken at very high gas fluxes in a range of 18 m/s < j_g < 37 m/s. The measured interfacial areas were very high. Values of up to 25 cm^2/cm^3 have been observed. Although some researchers have suspected these high values, the Wales data lie right on the extrapolated curves from Gregory and Scott's data as shown on Fig. 20. In view of the very high gas fluxes, the flow should have been in churn or annular-mist-flow regimes. Since the onset of entrainment velocity[67,68] is at about 14 m/s, a large portion of liquid should have been entrained as droplets in the gas stream. At the assumed droplet fraction of 0.1, the interfacial area of 10-25 cm^2/cm^3 requires the droplet diameter to be 0.25-0.7 mm.

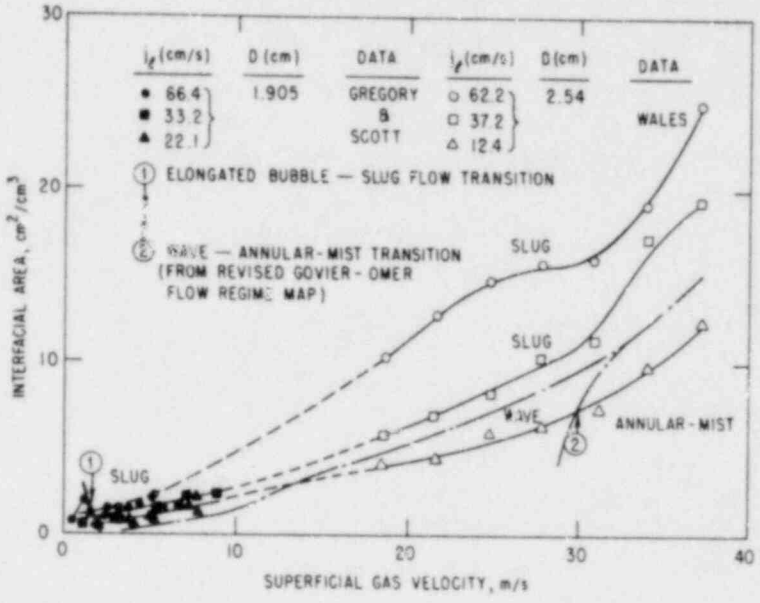

Fig. 20. Experimental Data of Interfacial Area at Relatively High Gas Volumetric Flux

The experiment of Wicks and Dukler[69] showed that the droplet diameter in annular flow of air and water was typically in a range of 0.1-0.7 mm. The data of Cousins and Hewitt[70] indicated that most droplets were in a range of 0.05-0.25 mm. Therefore, the estimated droplet diameter for the Wales experiment is in the same order of magnitude as those measured in other annular-flow experiments. From this it may be said that Wales correctly measured these very high interfacial areas for an annular-mist flow.

More data are available for interfacial areas; however, most of them are for special systems such as helical coils,[31,32] packed columns,[37,39] and agitated tanks.[33,34,36] Although these data can give some insight for understanding the effects of geometries and turbulences, they cannot be used as a data base for modeling a correlation for a straight tube.

V. INTERFACIAL-AREA CORRELATION DEVELOPMENT

A. Previous Work

There are some existing correlations for interfacial areas. Jepsen,[71] Banerjee,[31] and Kasturi[22] considered that the interfacial mass transfer or interfacial area is dependent on the dissipation in the fluid. This led them to correlate interfacial areas in terms of a frictional pressure drop and certain velocity scales. Thus,

$$a_i = f\left(\left[\frac{\partial p}{\partial z}\right]_{fr}, v\right). \tag{41}$$

Then a power relation between a_i and $[\partial p/\partial z]_{fr}$ or $v[\partial p/\partial z]_{fr}$ was assumed. By plotting data against these parameters in log-log scale, power and proportionality constants were obtained. However, the results were found to depend strongly on system geometries and possibly on the void fraction.[22] Both the power and proportionality constants changed considerably with system geometries. No models are available to calculate these constants without experimental data for that particular system. In other words, these existing correlations may be useful to rearrange data into a practical empirical correlation. However, the use of correlations cannot be extended to other systems.

From a physical point of view, there is no doubt that some relation exists between the frictional pressure drop and the interfacial area. Furthermore, there is a practical advantage for a chemical engineer to use the above correlation methods, because in most cases a simple prototypic experiment can be carried out to establish a necessary data base. However, for general two-phase-flow systems, the above-mentioned methods may not be suitable. Since the interfacial area concentration is a parameter that characterizes the structure of a flow, its mechanistic modeling should have been based on geometrical factors, void fraction, and flow. Note that the frictional pressure drop also depends on similar parameters. However, this does not justify the use of a direct relation between a_i and $[\partial p/\partial z]_{fr}$, such as Eq. 41. This mechanistic approach was first suggested by Ishii[1] and subsequently used by Saha[72] in his estimate of interfacial areas. In what follows, a preliminary correlation development based on the mechanistic approach is presented.

B. Dispersed Two-phase Flow

Basic parameters related to structures of two-phase flows, particularly of a dispersed flow, have already been discussed in Sec. II.A. These are the Sauter mean, drag, volume equivalent, and surface radii defined by Eqs. 9-12. These radii represent various length scales for a dispersed two-phase flow. Other macroscopic parameters are the void fraction, interfacial area concentration, and number density. Some of the important relations among these parameters are given by Eqs. 13-15. Therefore, the interfacial area per unit volume a_i becomes

$$a = \frac{3\alpha_d}{r_{sm}} = \frac{3\alpha_d}{r_v}\left(\frac{r_v}{r_{sm}}\right) = \frac{3\alpha_d}{r_v}\left(\frac{r_s}{r_v}\right)^2. \tag{42}$$

This equation shows that the interfacial area is a function of the void fraction, particle size, and shape factor. The particle size can be replaced by a number density N_d in view of Eqs. 11 and 12. Thus,

$$r_v = \left(\frac{3\alpha_d}{4\pi N_d}\right)^{1/3}. \tag{43}$$

Substituting Eq. 43 into Eq. 42, we obtain

$$a_i = 4.84\left(\frac{r_s}{r_v}\right)^2 N_d^{1/3}\alpha_d^{2/3}. \tag{44}$$

For an adiabatic flow, Eq. 42 is useful, because the size of the particles may be determined from initial and boundary conditions. For a two-phase flow with phase changes, Eq. 44 may be more convenient, because the sizes of particles change due to phase changes.

From Eqs. 42, 44, and 16, important shape factors for the interfacial terms are r_v/r_{sm}, r_s/r_v, and r_{sm}/r_D, which relate various length scales at interfaces. It is evident from the definitions that, for spherical particles,

$$\frac{r_v}{r_{sm}} = \frac{r_s}{r_v} = \frac{r_{sm}}{r_D} = 1. \tag{45}$$

However, the deviations of these shape factors from unity become significant as deformations of fluid particles increase in the distorted-particle and cap-bubble regimes.

For distorted particles, these shape factors may be correlated by Eotvos number,[64] defined by

$$N_{Eo} \equiv \frac{4g\Delta\rho r_v^2}{\sigma}. \tag{46}$$

Aspect ratio E, which is the ratio of the maximum vertical dimension to maximum horizontal dimension, can be given by the correlation of Wellek et al.[73] as

$$E = \frac{1}{1 + 0.163N_{Eo}^{0.757}}. \tag{47}$$

Note here that N_{Eo} is a function of only the particle size and properties. Therefore, by knowing the sizes of the particles, we can determine the aspect ratio.

By assuming an ellipsoidal shape, we can calculate various shape factors from simple geometric relations. For example,

$$\frac{r_v}{r_{sm}} = \frac{2 + \dfrac{E^2}{\sqrt{1 - E^2}} \ln \dfrac{1 + \sqrt{1 - E^2}}{1 - \sqrt{1 - E^2}}}{4E^{2/3}}, \tag{48}$$

where $E = b/r_p$ (see Fig. 21). And

$$\frac{r_{sm}}{r_D} = \frac{4}{2 + \dfrac{E^2}{\sqrt{1 - E^2}} \ln \dfrac{1 + \sqrt{1 - E^2}}{1 - \sqrt{1 - E^2}}}. \tag{49}$$

Under normal conditions, the aspect ratio E varies from 0.5 to 1. For these cases, only the shape factor for drag force is significantly different from unity. Other shape factors such as r_{sm}/r_v may be approximated as 1.

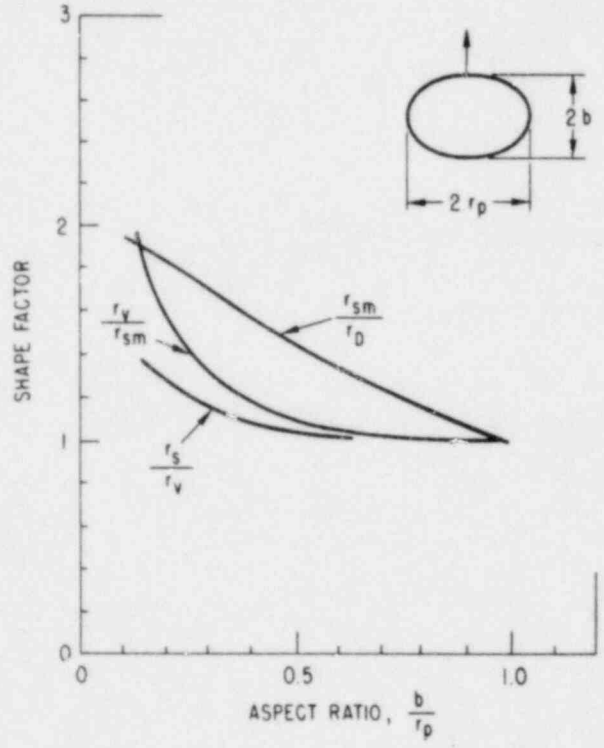

Fig. 21

Shape Factors for Ellipsoidal Particles

For the cap bubble shown in Fig. 22, the aspect ratio can be expressed in terms of the wake angle Θ as

$$E = \begin{cases} (1 - \cos\Theta)/2 \sin\Theta & \Theta < \frac{\pi}{2} \\ (1 - \cos\Theta)/2 & \Theta > \frac{\pi}{2}. \end{cases} \tag{50}$$

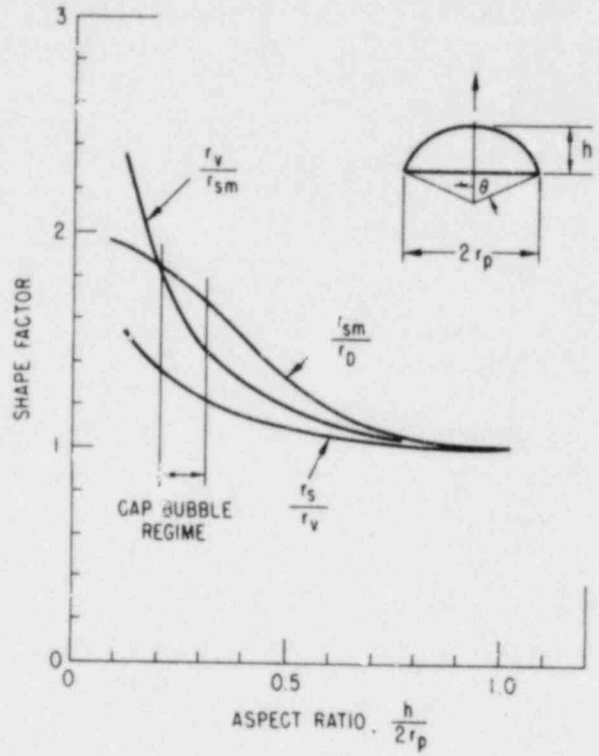

Fig. 22
Shape Factors for Cap Bubbles

Then from geometric considerations,

$$\frac{r_v}{r_{sm}} = \frac{3 + \cos\Theta}{[(1 - \cos\Theta)(2 + \cos\Theta)^2]^{1/3}} \tag{51}$$

and

$$\frac{r_{sm}}{r_D} = \begin{cases} 4(1 + \cos\Theta)/(3 + \cos\Theta) & \Theta < \frac{\pi}{2} \\ 4/(1 - \cos\Theta)(3 + \cos\Theta) & \Theta > \frac{\pi}{2}. \end{cases} \tag{52}$$

The results of Eqs. 50-52 are shown in Fig. 22. For cap bubbles, the wake angle is in the range of $46° < \Theta < 65°$.[74,75] This gives $1.4 < r_v/r_{sm} < 1.85$ and $1.65 < r_{sm}/r_D < 1.85$, which are considerably larger than unity.

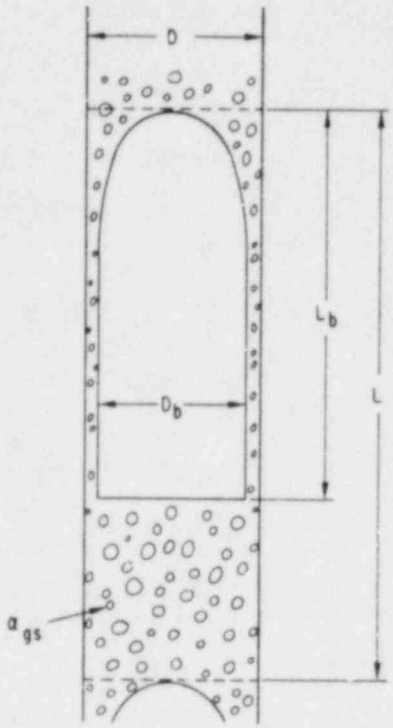

Fig. 23. Slug-flow Pattern

C. Slug and Churn-turbulent Flows

The slug-flow and churn-turbulent-flow regimes occur at an intermediate range of flow as transition regimes between a dispersed flow and a separated flow. A schematic of a slug flow used in the present analysis is shown in Fig. 23. The average overall void fraction is denoted by α, and the average void fraction in the liquid slug and film by α_{gs}. A typical element of a slug flow has a pitch of L and contains one large slug bubble and a number of small bubbles in the liquid slug and film. The diameter and length of a large bubble and the tube diameter are denoted by D_b, L_b, and D, respectively.

Then from a simple geometric consideration, the void fraction of a large slug bubble alone, α_b, in a total mixture is given by

$$\alpha_b = \frac{\alpha - \alpha_{gs}}{1 - \alpha_{gs}} = \left(\frac{D_b}{D}\right)^2 \frac{L_b - \frac{1}{6} D_b}{L}. \tag{53}$$

This implies that, in general, $\alpha > \alpha_{gs}$ for a slug flow and $\alpha = \alpha_{gs}$ corresponds to a bubbly flow. Now an interfacial area concentration can be calculated as

$$a_i = \frac{1}{D_b} \frac{\alpha - \alpha_{gs}}{1 - \alpha_{gs}} \frac{4 + D_b/L_b}{1 - D_b/6L_b} + \frac{1 - \alpha}{1 - \alpha_{gs}} \frac{3\alpha_{gs}}{r_{sm}}. \tag{54}$$

However, the ratio of the diameter to the length of a large slug bubble is almost always much less than 4, and the ratio of D_b to tube diameter D is approximately 0.88, as shown in Sec. VI.C below. The above equation can be given approximately by

$$a_i \simeq \frac{4.5}{D} \frac{\alpha - \alpha_{gs}}{1 - \alpha_{gs}} + \frac{3\alpha_{gs}}{r_{sm}} \frac{1 - \alpha}{1 - \alpha_{gs}}. \tag{55}$$

In view of Sec. V.2 above, r_{sm} may be replaced by the volume equivalent radius r_v in the above expression.

For churn-turbulent flow, the interfaces around the large bubbles become very irregular due to turbulent motions. To take account of this effect, a roughness parameter C_{ct} is introduced to modify Eq. 55 as

$$a_i \simeq \frac{4.5C_{ct}}{D} \frac{\alpha - \alpha_{gs}}{1 - \alpha_{gs}} + \frac{3\alpha_{gs}}{r_{sm}} \frac{1 - \alpha}{1 - \alpha_{gs}}, \tag{56}$$

where $C_{ct} > 1$. In general, however, the interfacial area concentration seems to decrease in churn-turbulent flow due to increased coalescence in the liquid-film and slug sections. In other words, C_{ct} acts to increase a_i, but a decrease in α_{gs} will reduce the overall value of a_i. These effects can be seen in Figs. 9-13.

D. Annular and Annular-mist Flows

An annular flow with droplet entrainment in the gas core is considered. The interfacial area for this annular-mist flow consists of two parts: film and droplets. Hence, from a simple geometric consideration,

$$a_i = \frac{4C_{an}}{D}\sqrt{\frac{\alpha}{1-\alpha_{fd}}} + \frac{\alpha}{1-\alpha_{fd}}\frac{3\alpha_{fd}}{r_{sm}}. \tag{57}$$

Here α, α_{fd}, and C_{an} denote the mean void fraction, the liquid-drop fraction in the gas core alone, and the roughness parameter due to waves in the film, respectively. Note that r_{sm} may be replaced by a shape factor and number density of droplets as shown in Sec. V.B. For most cases, however, for small droplets, $r_{sm} \simeq r_v$, where r_v is the volume equivalent radius.

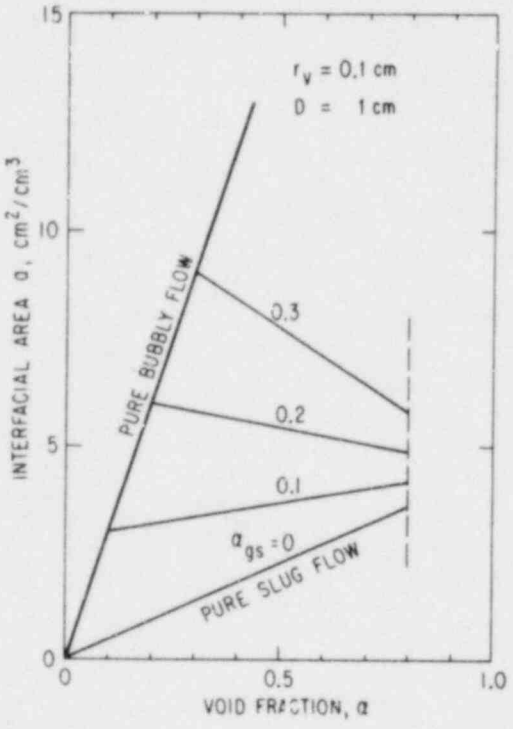

Fig. 24. Interfacial Area for Bubbly and Slug Flows

E. Relation to Experimental Data

The present model has not yet been compared directly to experimental data. This is because the interfacial area depends strongly on the existence and size of small fluid particles in all flow regimes as given by Eqs. 42, 55, 56, and 57. However, the sizes of these fluid particles have not been sufficiently analyzed to recommend the final correlations. Furthermore, most of the experimental data were taken with the volumetric fluxes as the expermental parameters. Relative velocity correlations should be used to recast these data in terms of the void fraction.

In spite of this, some sample calculations with estimated fluid-particle sizes gave correct experimental trends and correct orders of magnitude for interfacial areas (see Figs. 9-13, 24, and 25).

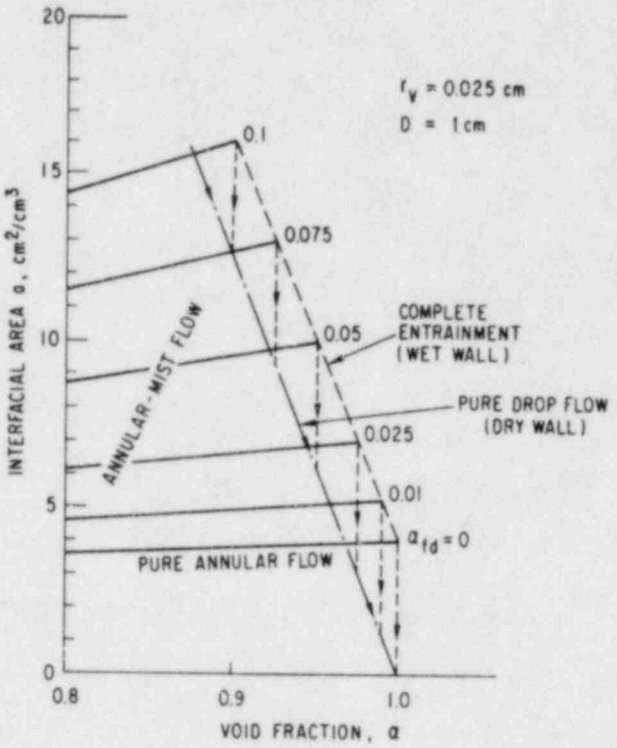

Fig. 25. Interfacial Area for Annular Flow

VI. FLOW-REGIME CRITERIA FOR TWO-FLUID MODEL

A. Requirement of Two-fluid Model

As discussed briefly in Sec. I, traditional flow-regime criteria based on volumetric fluxes[44-49] may not be suitable for a two-fluid-model formulation. This is because the geometrical parameters such as the void fraction cannot be determined uniquely by giving liquid and gas fluxes. In general, these parameters also depend on the slip or relative velocity between phases. The void fraction and interfacial area concentration characterize macroscopic geometric configurations of two-phase flows, namely, two-phase flow regimes. Therefore, the dependence of the void fraction not only on the volumetric fluxes, but also on the relative velocity, implies that the flow geometry may not be similar, even if j_g and j_f are the same.

This problem does not arise in steady-state and fully developed conditions, since, in these cases, relative velocity correlations can be used. Furthermore, even for certain transient problems, in which mixture models such as the drift-flux model are applicable, the use of the traditional flow-regime criteria is appropriate. This is consistent with the assumption that, for mixture models, relative motions between phases can be described by a constitutive relation rather than by a field equation.

However, this does not apply to rapid transient or entrance flows, where a two-fluid model becomes appropriate. Since the relative velocity is a variable to be solved from field equations in a two-fluid model, specifying the liquid and gas fluxes is insufficient for describing flow regimes. For a two-fluid-model formulation, the use of more direct geometric variables such as the void fraction and the interfacial area for flow-regime criteria appears to be practical and appropriate. In view of these observations, some modifications of conventional flow-regime criteria, as well as new flow-regime criteria using the void fraction as a parameter, have been studied.

B. Flow-regime Criteria for Unrestricted Systems

In an unrestricted two-phase-flow system, transitions between flow regimes occur when a drag law governing fluid-particle systems changes. Therefore the transition criteria can be obtained by matching the drag laws for the different regimes listed in Table I. From these drag correlations developed under the present study, the following transition criteria have been obtained.

1. Undistorted- to Distorted-particle (or Cap-bubble) Regime Transition

$$\frac{4r_v}{3}\sqrt{\frac{g\Delta\rho}{\sigma}} > \frac{24\left(1 + 0.1N_{Re}^{0.75}\right)}{N_{Re}}\left\{\frac{1 + 17.67[f(\alpha_d)]^{6/7}}{18.67 f(\alpha_d)}\right\}^2, \qquad (58)$$

where, for a bubbly flow, $f(\alpha_d) = (1 - \alpha_d)^{1.5}$ (see Table I). The above transition criterion can be approximated by

$$\frac{4r_v}{3}\sqrt{\frac{g\Delta\rho}{\sigma}} > (1 - \alpha_d)^{0.6}\,\frac{24(1 + 0.1N_{Re}^{0.75})}{N_{Re}}. \tag{59}$$

This criterion indicates the transition from the undistorted- to the distorted-particle regimes for $N_{Re} \geq 16$. However, for $N_{Re} < 16$, the same criterion indicates the transition to the cap-bubble regime directly.

2. Distorted-particle to Cap-bubble Regime Transition

$$\frac{4r_v}{3}\sqrt{\frac{g\Delta\rho}{\sigma}} > \frac{8}{3}(1 - \alpha_d)^{0.87}, \tag{60}$$

where an approximation similar to Eq. 59 has been used.

The above two results show that the effect of the void fraction on the regime transition is not very strong. The factors are $(1 - \alpha_d)^{0.6}$ and $(1 - \alpha_d)^{0.87}$, which range from 0.66 to 1 and from 0.55 to 1, respectively, for $0.5 < \alpha_d < 1$. The present criterion in the case of $\alpha_d = 0$ is compared to empirical results[64] for a single-particle system in Fig. 26. Note that the results shown by Clift et al.[64] are more conservative than the present model.

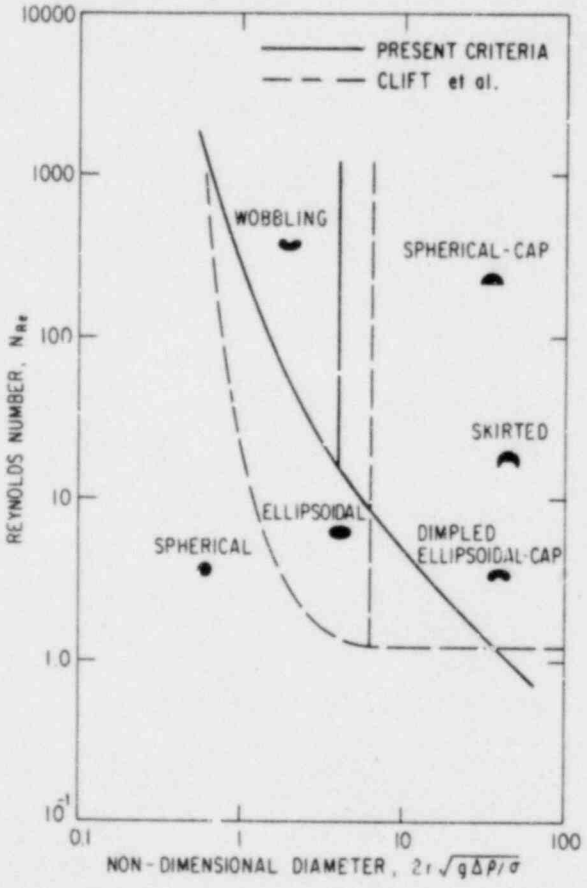

Fig. 26

Flow Regimes for Unrestricted Two-phase Flow

This can be explained by the fact that, in the present drag-law modeling, only undistorted- and distorted-particle regimes have been considered. Slight deformations corresponding to moderately ellipsoidal particles were considered insignificant in terms of the changes in the drag law; therefore, this regime was included in the undistorted regime. Except for this point, the agreement between the present correlation and the empirical results of Clift et al. is reasonably good at the zero void fraction.

C. Flow-regime Criteria for Restricted Systems

The discussion here is limited to a vertical system. Some results for a horizontal system have been given by Mishima and Ishii.[76]

1. Bubbly-flow to Slug-flow Transition

As studied by Radovich and Moissis[50] and Griffith and Snyder,[52] the transition from bubbly flow to slug flow occurs, mainly due to agglomerations of smaller bubbles into cap bubbles. Once a cap bubble is formed, further coalescences follow in the wake region of a cap bubble. This transition happens at the void fraction around 0.3. Radovich and Moissis[50] showed qualitatively that the probability of collisions becomes very large at $\alpha \approx 0.3$, and they postulated this as a cause of the flow-regime transition. Based on these observations, Dukler and Taitel[44] proposed $\alpha = 0.3$ as the criterion and then used a relative velocity correlation to convert it into a conventional form based on the volumetric fluxes of liquid and gas.

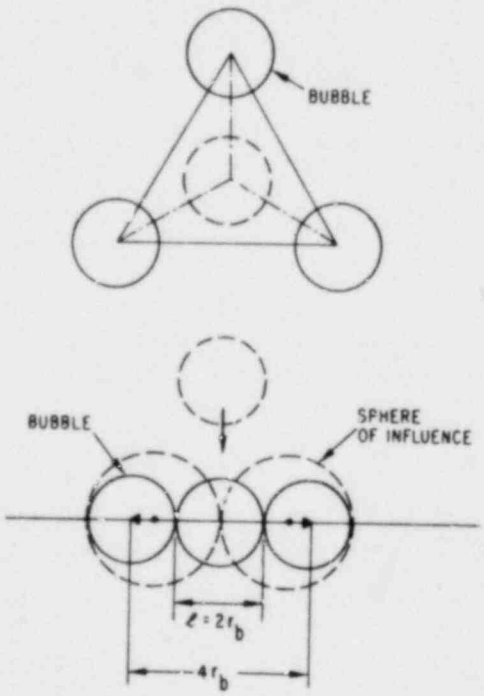

Fig. 27. Bubble Packing and Coalescence Pattern

The value of $\alpha = 0.3$ can also be obtained from a very simple geometrical consideration only. Suppose bubbles distribute themselves in a tetrahedral lattice pattern, in which each bubble fluctuates. It is assumed that there is a sphere of influence around each bubble. Although these spheres of influence can overlap in certain situations, the summation of the sphere volumes equals the total volume of the mixture. The number of not only the collisions but also the coalescences is considered to become very large if the maximum possible gap between two bubbles becomes less than a bubble diameter, as shown in Fig. 27. Under this condition, it is evident that the bubbles should deform considerably during each fluctuation. The above condition requires that

$$\alpha = \left(\frac{2}{3}\right)^3 = 0.296 \approx 0.3. \qquad (61)$$

2. Slug-flow to Churn-flow Transition

The transition is postulated to occur when the void fraction in the liquid-slug section reaches the void fraction at the slug-bubble section. In order to calculate the mean void fraction in the slug-bubble section, a potential flow analysis is applied to the film flow until the film flow along the bubble reaches the void fraction corresponding to the fully developed flow. Except very near the nose of the bubble, the application of the Bernoulli equation yields the local fraction to be

$$\alpha = \frac{\sqrt{2gh\Delta\rho/\rho_f}}{\sqrt{\frac{2gh\Delta\rho}{\rho_f}} + 0.2\left(1 - \sqrt{\rho_g/\rho_f}\right)j + 0.35\sqrt{\frac{\Delta\rho gD}{\rho_f}}}, \tag{62}$$

where h is the distance from the top of the bubble.

The slug-bubble length is obtained by equating the above α to the void fraction corresponding to the terminal film velocity. Hence the bubble length L_b becomes

$$\sqrt{\frac{2gL_b\Delta\rho}{\rho_f}} \simeq j + 0.75\sqrt{\frac{\Delta\rho gD}{\rho_f}}\left(\frac{\Delta\rho gD^3}{\rho_f\nu_f^2}\right)^{1/18}, \tag{63}$$

which is reasonably close to the experimental observation of Akagawa and Sakaguchi.[7] The mean void fraction at the slug-bubble section can be obtained from integrating Eq. 62 from 0 to L_b and dividing by L_b. Thus,

$$\alpha_m = 1 - 0.813\left[\frac{0.2\left(1 - \sqrt{\frac{\rho_g}{\rho_f}}\right)j + 0.35\sqrt{\frac{\Delta\rho gD}{\rho_f}}}{j + 0.75\sqrt{\frac{\Delta\rho gD}{\rho_f}}\left(\frac{\Delta\rho gD^3}{\rho_f\nu_f^2}\right)^{1/18}}\right]^{0.75}. \tag{64}$$

Since it is assumed that the transition from slug flow to churn flow occurs when the void fraction in the liquid-slug section reaches the mean void fraction in the slug-bubble section, the transition criterion is $\alpha > \alpha_m$.

3. Churn-flow to Annular-flow Transition

The criterion for this transition has been developed previously.[10] Therefore, for a small tube,

$$j_g\sqrt{\frac{\rho_g}{\Delta\rho gD}} > \alpha - 0.1 \text{ and } \alpha > \alpha_m. \tag{65}$$

However, for a large tube given by

$$D > \sqrt{\frac{\sigma}{\Delta\rho g}}\, N_{\mu f}^{-0.4}\Big/\left(\frac{1 - 0.1C_0}{C_0}\right)^2, \tag{66}$$

where

$$N_{\mu f} = \mu_f/(\rho_f \sigma \sqrt{\sigma/\Delta\rho g})^{1/2} \text{ and } C_0 = 1.2 - 0.2\sqrt{\rho_g/\rho_f}, \tag{67}$$

the criterion should be

$$j_g > \left(\frac{\sigma g \Delta\rho}{\rho_g^2}\right)^{1/4} N_{\mu f}^{-0.2}. \tag{68}$$

D. Comparison with Existing Criteria

The newly developed flow-regime criteria can be compared to some existing criteria[45-48] under steady-state and fully developed flow conditions. To transform the present criteria into the conventional form based on the volumetric fluxes, the relative velocity correlations of Ishii[10] have been used. In Fig. 28, the present criteria are compared to Govier and Aziz[46] and Griffith and Wallis,[47] and in Fig. 29 to Dukler and Taitel.[45] The agreement is reasonably good, except for the bubbly to slug transition criterion of Govier and Aziz.[46] Overall agreement between the present criteria and those of Dukler and Taitel is not surprising, because the basic principles involved in defining the transition criteria are similar.

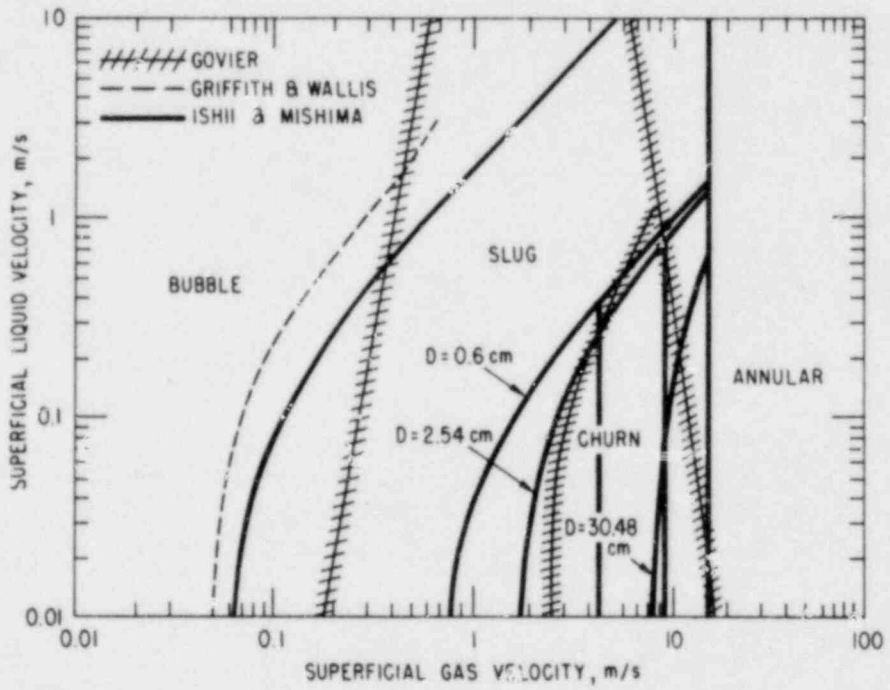

Fig. 28. Present Flow-regime Map Compared to Those of Govier and Aziz[46] and Griffith and Wallis[47]

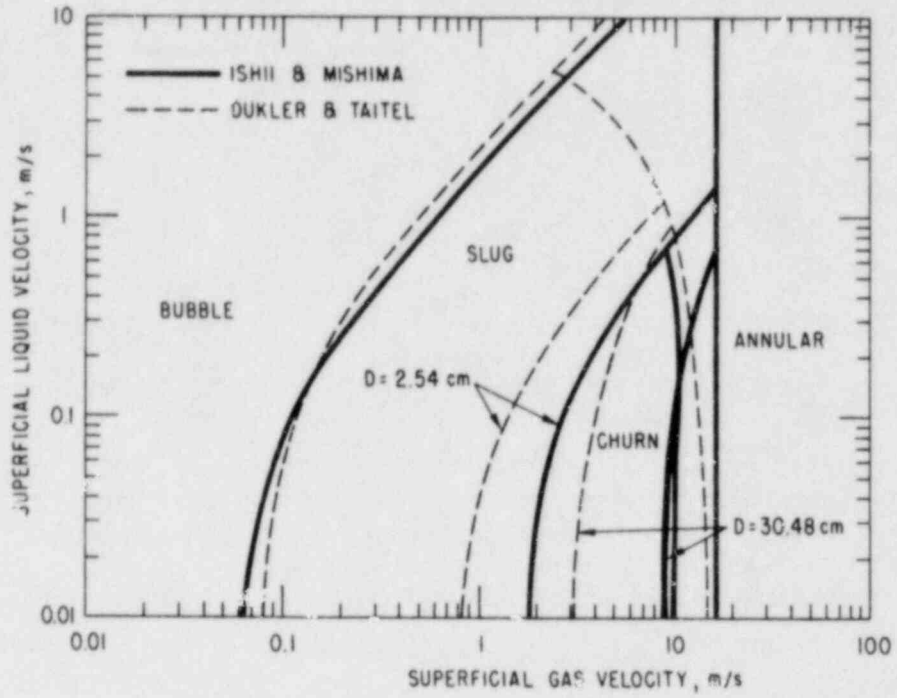

Fig. 29. Present Flow-regime Map Compared to That of Dukler and Taitel[45]

VII. SUMMARY AND CONCLUSIONS

The interfacial transfer terms for the two-fluid formulation have been studied in detail. The interfacial transfer of mass, momentum, and energy is proportional to the interfacial area and the driving force. These two effects are considered separately.

Geometrical effects on the interfacial transfers are taken into account primarily by the interfacial-area concentration. An extensive literature survey on existing experimental data has been completed, and a preliminary modeling effort for the interfacial area has been carried out. Basically four flow regimes--namely, dispersed (bubbly or droplet), slug, churn-turbulent, and annular flows--have been modeled separately, and general characteristics of the prediction have been discussed. The models show the importance of the existence and size of small fluid particles for all flow regimes.

Although a number of data exist, the ranges covered by these data are far short of being sufficient for reactor applications. The flows studied fell into the slug, churn, and annular-flow regimes at moderate liquid fluxes (3-50 cm/s). The range of the gas flux was 0.4-30 m/s. Note that no data exist for high liquid fluxes beyond 50 cm/s. The data for countercurrent or cocurrent down flows are completely missing. The diameters of tubes were relatively small (0.6-2.5 cm).

Furthermore, the effect of the density ratio or pressure on the interfacial areas has not been studied experimentally. However, the most important shortcoming of existing data may be the lack of information for developing flows. In view of fundamental difficulties encountered in modeling entrance and rapid transient flow under reactor accident conditions, considerable effort should be made to develop some data base for interfacial areas for such flows.

The modeling of the momentum interaction term is essentially completed. It was assumed that the general drag force can be expressed by a linear combination of three terms: the standard-drag, virtual-mass, and Basset forces. Each of these three forces is modeled separately. The standard-drag correlation was obtained from the postulated drag-similarity law based on the mixture viscosity. The results for dispersed, slug, and churn-turbulent flows were compared to over 1000 data. Satisfactory agreements were obtained at wide ranges of concentration and Reynolds number.

Traditional flow-regime criteria based on the vapor and liquid volumetric fluxes are not suitable to the two-fluid-model formulation, because these two parameters do not determine the void fraction uniquely. It has been concluded that for a two-fluid model, direct geometrical parameters such as the void fraction and interfacial area should be used in flow-regime criteria. From this point of view, new flow-regime criteria for both unrestricted and restricted flows have been developed. These new criteria can be compared to existing criteria under steady-state and fully developed flows by using relative velocity correlation obtained previously. The results showed satisfactory agreements.

For rapid transient and entrance flow, even these new flow-regime criteria may not be sufficient. In such flows, the flow regimes as well as the interfacial-area concentration can be very sensitive to initial conditions and relaxation processes. The mechanism of coalescences and disintegrations of fluid particles becomes essential in these situations. The most general method to include these effects is to introduce a transport equation for the interface area. However, basic experimental data needed to develop this model have been found to be grossly inadequate. Therefore, it is recommended that such experiments should be performed.

ACKNOWLEDGMENTS

We would like to express our appreciation to Drs. N. Zuber and Y. Y. Hsu of NRC for valuable discussions on the subject.

The work was performed under the auspices of the U. S. Nuclear Regulatory Commission.

REFERENCES

1. M. Ishii, *Thermo-fluid Dynamic Theory of Two-phase Flow*, Eyrolles, Paris (1975).

2. J. M. Delhaye, *Equations fondamentales des écoulements diphasiques, Parts 1 and 2*, CEA-R-3429, France (1968).

3. P. Vernier and J. M. Delhaye, *General Two-phase Flow Equations Applied to the Thermohydrodynamics of Boiling Nuclear Reactor*, Energ. Prim. 4(1) (1968).

4. J. Bouré and M. Réocreux, "General Equations of Two-phase Flows," *4th All Union Heat and Mass Transfer Conference*, Minsk, USSR (1972).

5. G. Kocamustafaogullari, *Thermo-fluid Dynamics of Separated Two-phase Flow*, Ph.D. thesis, School of Mechanical Engineering, Georgia Institute of Technology, Georgia (1971).

6. T. C. Chawla and M. Ishii, *Two-fluid Model of Two-phase Flow in a Pin Bundle of a Nuclear Reactor*, ANL/RAS/LWR 79-5 (1979).

7. A. A Amsden and F. H. Harlow, *K-TIF: A Two-fluid Computer Program for Downcomer Flow Dynamics*, LA-6994 (1978).

8. M. I. Thurgood et al., *Core Thermal Model Development*, PNL-2653-2, NUREG/CR-0341, p. 101 (1978).

9. N. Zuber, "Flow Excursions and Oscillations in Boiling, Two-phase Flow Systems with Heat Addition," in *Proceedings of EURATOM Symposium on Two-phase Flow Dynamics*, Commission of European Communities, Brussels *1*, pp. 1070-1089 (1967).

10. M. Ishii, *One-dimensional Drift-flux Model and Constitutive Equations for Relative Motion between Phases in Various Two-phase Flow Regimes*, ANL-77-47 (1977).

11. R. T. Lahey, Jr., L. Y. Cheng, D. A. Drew, and J. E. Flaherty, "The Effect of Virtual Mass on the Numerical Stability of Accelerating Two-phase Flows," presented at *AIChE 71th Annual Meeting at Miami Beach, Florida (1978)*.

12. *M. Réocreux, Contribution á l'étudedes debits critiques en écoulement diphasique eau vapeur*, Ph.D. thesis, University of Grenoble, France (1974), also NUREG-tr-0002, Vol. 1.

13. N. Zuber, *On the Dispersed Two-phase Flow in the Laminar Flow Regime*, Chem. Eng. Sci. *19*, p. 897 (1964).

14. M. Ishii and N. Zuber, *Drag Coefficient and Relative Velocity in Bubbly, Droplet or Particulate Flows*, AIChE J. *25*, 843 (1979).

15. M. Ishii and N. Zuber, "Relative Motion and Interfacial Drag Coefficient in Dispersed Two-phase Flow of Bubbles, Drops or Particles," *71st Am. Inst. of Chem. Engrs. Annual Meeting*, Miami (1978).

16. M. Ishii and T. C. Chawla, *Local Drag Laws in Dispersed Two-phase Flow*, ANL-79-105, NUREG/CR-1230 (1979).

17. M. Ishii and T. C. Chawla, "Two-fluid Model and Momentum Interaction between Phases," *NRC 7th Water Reactor Safety Research Information Meeting*, Gaithersburg (Nov 1979).

18. M. M. Sharma and R. A. Mashelkar, "Absorption with Reaction in Bubble Columns," Inst. of Chem. Engrs., Symposium Series *28, Tripartite Chemical Engineering Conference*, Montreal (1968).

19. A. P. Watson, D. E. Cormack, and M. E. Charles, *A Preliminary Study of Interfacial Areas in Vertical Cocurrent Two-phase Upflow*, Can. J. Chem. Eng. *57*, p. 16 (1979).

20. R. V. Shilimkan and J. B. Stepanek, *Interfacial Area in Cocurrent Gas-Liquid Upward Flow in Tubes of Various Size*, Chem. Eng. Sci. *32*, 149 (1977).

21. K. Akita and F. Yoshida, *Bubble Size, Interfacial Area, and Liquid-phase Mass Transfer Coefficient in Bubble Columns*, Ind. Eng. Chem. Process cess Des. Dev. *13*(1), 84 (1974).

22. G. Kasturi and J. B. Stepanek, *Two-phase Flow-III. Interfacial Area in Cocurrent Gas-Liquid Flow*, Chem. Eng. Sci. *29*, 713-719 (1974).

23. K. Bier et al., *Blasenbildung und Phasengrenzfläche beim Dispergieren von Gasen in Flüssigkeiten an einzelnen Gaszulauföffnungen, Teil 2: Einflutz von Systemdruck und Stoffeigenschaften auf die Blasengröbe und die spezifische Phasengrenzfläche*, Wärme-und Stoffübertragung *11*, 217 (1978).

24. G. A. Gregory and D. S. Scott, "Physical and Chemical Mass Transfer in Horizontal Cocurrent Gas-Liquid Slug Flow," *Proceedings of Int. Symp. on Res. in Cocurrent Gas-Liquid Flow*, Waterloo (1968).

25. A. K. Shah and M. M. Sharma, *Mass Transfer in Gas-Liquid (Horizontal) Pipeline Contactors*, Can. J. Chem. Eng. *53*, 572 (1975).

26. C. E. Wales, *Physical and Chemical Absorption in Two-phase Annular and Dispersed Horizontal Flow*, AIChE J. *12*(6), 1166 (1966).

27. K. E. Porter, M. B. King, and K. C. Varshney, *Interfacial Areas and Liquid-Film Mass-Transfer Coefficients for a 3 ft. Diameter Bubble Cap Plate Derived from Absorption Rates of Carbon Dioxide into Water and Caustic Soda Solutions*, Trans. Inst. Chem. Eng. *44*, T27½ (1966).

28. G. B. Dillion and I. J. Harris, *The Determination of Mass Transfer Coefficients and Interfacial Areas in Gas-Liquid Contacting Systems*, Can. J. Chem. Eng. *44*, 307 (1966).

29. H. K. Abdel-Aal, G. B. Stiles, and C. D. Holland, *Formation of Interfacial Area at High Rates of Gas Flow through Submerged Orifices*, AIChE J. *12*(1), 174 (1966).

30. J. M. Burgess and P. H. Calderbank, *The Measurement of Bubble Parameters in Two-phase Dispersions--II, The Structure of Sieve Tray Froths*, Chem. Eng. Sci. *30*, 1107 (1975).

31. S. Banerjee, D. S. Scott, and E. Rhodes, *Studies on Cocurrent Gas-Liquid Flow in Helically Coiled Tubes, II. Theory and Experiments on Turbulent Mass Transfer with and without Chemical Reaction*, Can. J. Chem. Eng. *48*, 542 (1970).

32. E. Kulic and E. Rhodes, *Chemical Mass Transfer in Co-Current Gas-Liquid Slug Flow in Helical Coils*, Can. J. Chem. Eng. *52*, 114 (1974).

33. C. W. Robinson and C. R. Wilke, *Simultaneous Measurement of Interfacial Area and Mass Transfer Coefficients for a Well-mixed Gas Dispersion in Aqueous Electrolyte Solutions*, AIChE J. *20*(2), 285 (1974).

34. T. Sridhar and O. E. Potter, *Interfacial Area Measurements in Gas-Liquid Agitated Vessels--Comparison of Techniques*, Chem. Eng. Sci. *33*, 1347 (1978).

35. K. Sridharan and M. M. Sharma, *New Systems and Methods for the Measurement of Effective Interfacial Area and Mass Transfer Coefficients in Gas-Liquid Contactors*, Chem. Eng. Sci. *31*, 767 (1976).

36. V. D. Mehta and M. M. Sharma, *Mass Transfer in Mechanically Agitated Gas-Liquid Contactors*, Chem. Eng. Sci. *26*, 461 (1971).

37. B. W. Shende and M. M. Sharma, *Mass Transfer in Packed Columns: Cocurrent Operation*, Chem. Eng. Sci. *29*, 1763 (1974).

38. M. M. Sharma and R. K. Gupta, *Mass Transfer Characteristics of Plate Columns without Downcomer*, Trans. Inst. Chem. Eng. *45*, T169 (1967).

39. R. A. Mashelkar and M. M. Sharma, *Mass Transfer in Bubble and Packed Bubble Columns*, Trans. Inst. Chem. Eng. *48*, T162 (1970).

40. M. M. Sharma and P. V. Danckwerts, *Chemical Methods of Measuring Interfacial Area and Mass Transfer Coefficients in Two-fluid Systems*, Br. Chem. Eng. *15*(4), 522 (1970).

41. V. G. Trice, Jr., and W. A. Rodger, *Light Transmittance as a Measure of Interfacial Area in Liquid-Liquid Dispersions*, AIChE J. *2*(2), 205 (1956).

42. J. Landau et al., *Comparison of Methods for Measuring Interfacial Areas in Gas-Liquid Dispersions*, Can. J. Chem. Eng. *55*, 13 (1977).

43. P. H. Calderbank, *Physical Rate Processes in Industrial Fermentation, Part I and Part II*, Trans. Inst. Chem. Eng. *36*, 443 (1958) and *37*, 173 (1959).

44. A. E. Dukler and Y. Taitel, *Flow Regime Transitions for Vertical Upward Gas Liquid Flow: A Preliminary Approach Through Physical Modeling, Progress Report No. 1*, NUREG-0162 (1977).

45. A. E. Dukler and Y. Taitel, *Flow Regime Transitions for Vertical Upward Gas Liquid Flow, Progress Report No. 2,* NUREG-0163 (1977).

46. G. W. Govier and K. Aziz, *The Flow of Complex Mixtures in Pipes,* Van Nostrand Reinhold, New York (1972).

47. P. Griffith and G. B. Wallis, *Two-phase Slug Flow,* J. Heat Trans. *83C*(3), 307 (1961).

48. A. E. Bergles, J. P. Roos, and J. G. Bourne, *Investigation of Boiling Flow Regimes and Critical Heat Flux,* AEC Report NYO-3304-13 (1968).

49. C. L. Williams and A. C. Peterson, Jr., *Flow Patterns in High Pressure Two-phase Flow--A Visual Study of Water in a Uniformly Heated 4-Rod Bundle,* WAPD-TM-1199 (1975).

50. N. A. Radovich and R. Moissis, *The Transition from Two-phase Bubble Flow to Slug Flow,* MIT Report No. 7-7633-22 (1962).

51. P. H. Calderbank, M. B. Moo-Young, and R. Bibby, "Coalescence in Bubble Reactors and Absorbers," *3rd European Symp. on Chem. Reaction Eng.,* Amsterdam (1964).

52. P. Griffith and G. A. Snyder, *The Bubbly-Slug Transition in a High Velocity Two-phase Flow,* MIT Technical Report No. 5003-29 (1964).

53. T. Otake et al., *Coalescence and Breakup of Bubbles in Liquids,* Chem. Eng. Sci. *32,* 377 (1977).

54. S. Narayanan, L. H. J. Goossens, and N. W. F. Kossen, *Coalescence of Two Bubbles Rising in Line at Low Reynolds Numbers,* Chem. Eng. Sci. *29,* 2071 (1974).

55. Noel de Nevers and Jen-Liang Wu, *Bubble Coalescence in Viscous Fluids,* AIChE J. *17*(1), 182 (1971).

56. E. Kojima, T. Akehata, and T. Shirai, *Behavior of Single Air Bubbles Held Stationary in Downward Flows,* J. Chem. Eng. Jpn. *8*(2), 108 (1975).

57. F. C. Yip, J. E. S. Vernart, and G. W. Govier, *The Motion of Small Air Bubbles in Stagnant and Flowing Water,* Can. J. Chem. Eng. *48,* 229 (1970).

58. R. Moissis and P. Griffith, *Entrance Effects in a Two-phase Slug Flow,* Trans. ASME, J. Heat Transfer *84,* 29 (Feb 1962).

59. I. A. Morrison, *Breakup of a Bubble Chain,* Chem. Eng. Sci. *28,* 1115 (1973).

60. G. D. M. MacKay and S. G. Mason, *The Gravity Approach and Coalescence of Fluid Drops at Liquid Interfaces,* Can. J. Chem. Eng. *41,* 203 (1963).

61. T. E. Ramabhadran, T. W. Peterson, and J. H. Seinfeld, *Dynamics of Aerosol Coagulation and Condensation,* AIChE J. *22*(5), 840 (1976).

62. T. E. Ramabhadran, C. H. Byers, and J. C. Friedly, *On the Dynamics of Fluid Interfaces,* AIChE J. *22*(5), 872 (1976).

63. J. M. Delhaye and J. L. Achard, "On the Use of Averaging Operators in Two-phase Flow Modeling," *ASME Symp. on Thermal and Hydraulic Aspects of Nuclear Reactor Safety 1, Light Water Reactors,* Atlanta (1977).

64. R. Clift, J. R. Grace, and M. E. Weber, *Bubbles, Drops, and Particles,* Academic Press, New York (1978).

65. L. M. Milne-Thomson, L. M., *Theoretical Hydrodynamics,* MacMillan, New York (1963).

66. Yu. G. Mokeyev, *Effect of Particle Concentration on Their Drag and Induced Mass,* Fluid Mech. Sov. Res. *6,* 161 (1977).

67. M. Ishii and M. A. Grolmes, *Inception Criteria for Droplet Entrainment in Two-phase Concurrent Film Flow,* AIChE J. *21*(2), 308 (1975).

68. G. F. Hewitt and N. S. Hall-Taylor, *Annular Two-phase Flow,* Pergamon Press, Oxford (1970).

69. M. Wicks and A. E. Dukler, "In situ Measurements of Drop Size Distribution in Two-phase Flow," *Int. Heat Transfer Conf.,* Chicago (1966).

70. L. B. Cousins and G. F. Hewitt, *Liquid Mass Transfer in Annular Two-phase Flow,* AERE-R5657 (1968).

71. J. C. Jepsen, *Mass Transfer in Two-phase Flow in Horizontal Pipelines,* AIChE J. *16*(5), 705 (1970).

72. P. Saha, *Light Water Reactor Thermal/Hydraulic Development Program, 1.1 Development of Constitutive Relations, 1.1.1. Analytical Modeling, (b) Effect of Pressure Change,* BNL-NUREG-50683, p. 145 (1977).

73. R. M. Wellek, A. K. Agrawal, and A. H. P. Skelland, *Shape of Liquid Drops Moving in Liquid Media,* AIChE J. *12*(5), 854 (1966).

74. R. M. Davies and G. Taylor, *The Mechanics of Large Bubbles Rising through Extended Liquids and through Liquids in Tubes,* Proc. Roy. Soc. London *A200,* 375 (1950).

75. T. Z. Harmathy, *Velocity of Large Drops and Bubble in Media of Infinite or Restricted Extent,* AIChE J. *6*(2), 281 (1960).

76. K. Mishima and M. Ishii, *Theoretical Prediction of Onset of Horizontal Slug Flow,* J. Fluid Eng. *102*, 441 (1980).

77. K. Akagawa and T. Sakaguchi, *Fluctuation of Void Ratio in Two-phase Flow,* Bull. Jpn. Soc. Mech. Eng. *9*, 105 (1966).

Distribution for NUREG/CR-1873 (ANL-80-111)

Internal:

E. S. Beckjord
C. E. Till
R. Avery
J. F. Marchaterre
A. J. Goldman
P. A. Lottes
L. W. Deitrich
D. Rose
R. H. Sevy
I. Bornstein
D. H. Cho
P. B. Abramson
D. P. Weber
W. T. Sha
Y. W. Shin
D. M. France
W. L. Chen
J. C. Leung
T. C. Chawla
H. U. Wider
M. Ishii (21)
ANL Contract File
ANL Libraries (2)
TIS Files (6)

External:

NRC Washington, for distribution per R2 and R4 (455)
DOE-TIC (2)
Manager, Chicago Operations and Regional Office, DOE
Chief, Office of Patent Counsel, DOE-CORO
President, Argonne Universities Association
Reactor Analysis and Safety Division Review Committee:
S. Baron, Burns and Roe, Inc., 700 Kinderkamack Rd., Oradell, N. J. 07649
J. R. Dietrich, 165 Wood Pond Rd., West Hartford, Conn. 06107
L. C. Hebel, Xerox Corp., 3333 Coyote Hill Rd., Palo Alto, Calif. 94304
W. Kerr, U. of Michigan, Ann Arbor, Mich. 48109
S. Levine, NUS Corp., 4 Research Pl., Rockville, Md. 20850
S. Levy, S. Levy, Inc., 1901 S. Bascom Ave., Campbell, Calif. 95008
D. Okrent, U. of California, Los Angeles, Calif. 90024